AZERBAIJANI ASTRONOMICAL JOURNAL

Kuznetsov V.D.
Pushkov Institute of Terrestrial Magnetism,
Ionosphere and Radio Wave Propagation of Russian
Academy of Sciences, Russian Federation
Cherepaschuk A.M.
Lomonosov Moscow State University,
Russian Federation
Bakısh V.
Akdeniz University, Turkey
Samadov Z.A.
Baku State University Department of Astrophysics
Huseynov N.A.
Shamakhy Astrophysical Observatory
Alisheva K.I.
Baku State University Department of Astrophysics
Rustamov J.N.
Shamakhy Astrophysical Observatory
Gasimov H.A.
Baku Engineering University

AZERBAIJANI ASTRONOMICAL JOURNAL

2025, Vol. 20, № 1

Contents

)

REVISITING BOLOMETRIC CORRECTIONS: OLDER AND NEWER USAGES

Z. Eker [a*]

[a] *Akdeniz University, Faculty of Sciences, Dept. of Space Sciences and Technologies, Kampüs, Dumlupınar cd., Pınarbaşı mah., Antalya, Türkiye*

The concept of bolometric magnitude, introduced by Eddington in 1926, represented stellar luminosity for theoretical mass-luminosity studies, complementing photographic and visual magnitudes. Bolometric correction (BC), defined as BC = M_{bol} - M_v = $m_{bol} - m_v$, became a crucial tool in the 20th century for calibrating stellar temperature scales, particularly when only B-V (photographic - visual) color indices were available. Despite advancements in multi-color photometry, classical BC usage persisted, leading to misconceptions: that BC must always be negative, bolometric magnitudes are inherently brighter than visual, and BC zero-points are arbitrary. These were clarified with IAU's 2015 GAR B2 resolution, which established a consistent zero-point, revealing BC's potential for accurately determining stellar luminosities. This study revisits the evolution of BC, addressing its historical and modern usage, and demonstrates how multi-color photometry combined with BC enables precise stellar luminosity measurements, accurate to a few percent.

Keywords: Stars: fundamental parameters; stars: general; solar and stellar astrophysics; astrophysics - instrumentation and methods for astrophysics

1. INTRODUCTION

The bolometric correction (BC) of a star is defined as the difference between its bolometric and visual magnitudes. This definition is first given by [26] as

$$BC = M_{bol} - M_{pv} = m_{bol} - m_{pv} \qquad (1)$$

if

$$M_{bol} = M_{bol}(sun) - 2.5logL \qquad (2)$$

where the subscripts bol and pv indicate bolometric and photovisual, M and m are absolute and apparent magnitudes while L is the luminosity of the star in solar units. This definition is commonly accepted and used throughout of the century and even today, thus astronomers handbook "Allen's Astrophysical Quantities" [9] retained the same definition as "BC=bolometric correction=m_{bol}-V" with a note "always negative". If equation (1) is arranged as M_{bol}=M_V+BC and m_{bol}=V+BC, the term BC could be interpreted as the correction added to the visual magnitudes. There is no telescope nor a detector to observe a star at all wavelengths, thus the missing part, named BC, must be added to the observable magnitude (nowadays, could be at any band of any photometric system) in order to obtain the bolometric magnitude, which represents hypothetical brightness of the star at all wavelengths from zero to infinity.

This definition of BC, which has been used since [26], has chronic problems which [13] and [15] call them paradigms: 1) BC of a star must always be negative, 2) Bolometric magnitude of a star ought to be brighter than its V magnitude, 3) The zero point of BC scale is arbitrary. On the contrary, without recognizing them as paradigms, [36] says "Note that this definition is usually interpreted to imply that the bolometric corrections must always be negative, although many of the currently used tables of empirical BC_V values violate this condition" for the problem one, "bolometric magnitude of a star ought to be brighter than its V magnitude according to equation (1)" for the problem two and writing the Kuiper's definition (equation 1) in the integral form for the V band BC

$$BC_V = 2.5log(\int_0^\infty S_\lambda(V)f_\lambda d\lambda / \int_0^\infty f_\lambda d\lambda) + C_2, \qquad (3)$$

where S_λ (V) is the sensitivity function for the V magnitude system, "the constant C_2 contains an arbitrary zero point that has been a common source of confusion" for problem three as if defending them as natural problems solvable by using the correct values of M_{bol} and BC_V for the Sun. Actually, the problem is much bigger than [36] imagined. As it was described by [13], there are two schools of thought that treat the arbitrariness of the BC scale differently. One school [9, 21, 22, 26, 28, 29, 31, 37] intentionally and knowingly shifts computed BC values to make them all negative, that is, obeys all of the three paradigms, while the other school [5, 6, 8, 12, 17, 18, 23, 24, 35] prefers retaining BC values as computed, even if there are positive BC values.

The first group appears self-consistent according to the paradigms. However, the second group, which retains the BC values as they are, even if there are positive values, ignores the note 'BC = m_{bol} - V (always negative)' (page 381 in [9])

or a positive BC is not seen as a violation. It is not possible for both schools to be consistent.

It is obvious that a positive BC (BC > 0), according to paradigms 1 and 2, is a serious problem according to the first school because a positive BC implies L_V, an observable part of the luminosity of a star corresponding to M_v, greater than its total luminosity L. This, however, is unphysical as if a part of a unit is greater than the unit itself. But on the other hand, according to the second school, the arbitrariness of the zero-point constant of the BC scale, which gives freedom to the first school to shift their BC numbers until all BC values are negative, is another dead end. This is because, for every other arbitrary value of C_2 in equation (3), there must be another BC_V. For every other value of BC_V, there must be another M_{bol} for the star having an M_v according to the original definition of BC by [26] (equation 1). Then, despite M_v is the single entity, every other value of M_{bol} implies the star has many different values of L according to equation (2). How can a single star, with a single M_v, have many different values of L as many as the number of arbitrary zero-point constants which could be used by different users. Arbitrariness implies a single star would have an infinite number of different L, which is also unphysical. Although the problems appear solvable according to [36], the current definition and usages of BC are so ill-posed that there could be no solution et al, in other saying, there is a crisis in the development of BC, as described by [27].

According to [27], who is one of the most distinguished philosophers of science in the twentieth century, science does not progress linearly. Science progresses through revolutions. Between the revolutions is called the period of normal science in which scientists work under dominant paradigm(s), thus, anomalies were ignored. By the time anomalies increase, become intolerable, then a crisis emerges. The crisis was overcome by a revolution, then a new normal science period with new paradigm(s) will start. The purpose of this study is to investigate the pre-science period in the development line of BC search for the origins of the three paradigms and then pronounce the silent revolution [15], that is, how the misleading three paradigms were already broken; meanwhile, older and newer usages of BC will be described automatically.

2. EARLY CONCEPTS OF BC AND ORIGINS OF THE PARADIGMS

2.1. Luminous Efficiency

The earliest concept of BC was introduced by Eddington [10], who called it "luminous efficiency" as an auxiliary parameter when he was upgrading mass-absolute magnitude relation dicovered independently by [20] and [33]. These were

the times in the history of science when the stellar temperature scale just recently (a decade ago) established by the spectral sequence and used in the newly established H-R diagrams by [19] and [32] in 1913. The primary purpose of [10] was to formulate a theoretical mass-luminosity relation, which retained absolute bolometric magnitude (M_{bol}) to indicate luminosity of a star against its mass. In these years, there were only three types of magnitudes: visual (M_v), photographic (M_p), and bolometric (M_{bol}) until the three color (UBV) photometry was introduced by Johnson and Morgan [25]. M_{bol} was chosen because the other two magnitudes were not suitable to represent total radiation of a star. Rather than being a hypothetical brightness to indicate luminosity of a star, the bolometric magnitude was just another observable quantity for Eddington and his colleagues who could obtain it by an instrument such as a bolometer, a radiometer or a galvanometer. Eddington commented:

"It is now practical to measure the heat received from a star by the use of a radiometer. Considerable sensitiveness in the method has been developed (It is said that the equipment at Mount Wilson could detect the heat of a candle on the banks of the Mississippi). But the results attained are as yet very limited and in general we have to infer the total amount of heat emitted from the light emitted (the deduction of bolometric magnitude from heat measurement is not really more direct than from light measurement, because large corrections must be applied on account of atmospheric absorption in the infra-red, and this involves assuming a spectral energy distribution just as the reduction of light measurements does). This involves of the luminous efficiency of the energy emitted by stars of different types."

and gave the definition of the luminous efficiency of a star with an effective temperature T_e as

$$< P > = \frac{\int p(\lambda) I'(\lambda, T_e) d\lambda}{I'(\lambda, T_e) d\lambda} \tag{4}$$

where $I'(\lambda, T_e)$ is the black body intensity at a wavelength λ and $p(\lambda)$ is the factor for the luminous efficiency thus $<P>$ is the mean value of it for a star with T_e. Since nuclear reactions such as p-p chain and CNO cycle were not discovered, Eddington was assuming stars are hot spheres of gases. According to Eddington the maximum of $<P>$ occurs for the stars of types F to G, presumably, that is because our visual sense has been developed respect to sunlight. Eddington continued *"It is convenient to take the maximum as standard, and to define the scale of bolometric magnitude at this effective temperature. At any other temperature P will be smaller and the star will be brighter bolometrically than visually"*.

Readers should pay attention to the last sentence, which is nothing but the first verbal expression of the second paradigm. In fact, the definition of luminous efficiency resembles the definition of BC according to equation (3) if one replaces

Table 1. Effective temperatures, luminous efficiency (p) and magnitude difference between bolometric and visual (Eddington 1926).

T_e (K)	p	Δm (Vis.-bol.)
		m
2540	0.092	+2.59
3000	0.206	+1.71
3600	0.417	+0.95
4500	0.723	+0.35
6000	1.000	0.00
7500	0.985	+0.02
9000	0.893	+0.12
10500	0.749	+0.31
12000	0.616	+0.53

$p(\lambda)$ with S_λ (V) and black body intensity $I'(\lambda, T_e)$ with the black body flux f_λ. Thus, the luminous efficiency of the human eye acts like the visual filter in the three color (UBV) photometry. The only difference is that the luminous efficiency is without an arbitrary constant as in equation (3).

Eddington gave a table (Table 1) for those who would have the star's visual magnitude but not its bolometric magnitude. Knowing T_e and the star's visual magnitude, one can estimate its apparent bolometric magnitude (Table 1). If the star's parallax is also available, one can get its absolute bolometric magnitude. At last, using the mass-luminosity relation of Eddington, the mass of the star could be obtained. Apparently, Eddington solved a very crucial problem of estimating masses of single stars for which Kepler's third law is not applicable.

2.2. Heat-index

Apparently, the term "luminous efficiency" did not thrill the successors of Eddington. First, [30] preferred to use the term "heat-index", which they define it as the difference between visual minus radiometric magnitudes of a star. Remembering that the radiometers were used for measuring the heat received from a star, and bolometric magnitudes also come from radiometers, then it is more meaningful to call the difference between visual and bolometric "heat-index" which is essentially the same quantity displayed in the third column of Table 1. The third column of Table 1, however, is nothing but the ten-based logarithm of the second column (luminous efficiency). If the ten-based logarithm of the luminous effi-

ciency is multiplied by 2.5, then it is called "heat-index". [30] gave the following formula for one to obtain the apparent bolometric magnitude of a star from its radiometric magnitude,

$$m_b = m_r - \Delta m_r + (H.I. + \Delta m_r)_s \qquad (5)$$

where $(H.I.+\Delta m_r)_s$ was defined as the heat-index plus the reduction to no atmosphere for the particular star or class of stars for which the radiometric and bolometric scales were made to coincide. The "radiometric magnitude" of a star, however, was defined as equal to the apparent magnitude of an A0 star which will give the observed galvanometer deflection. [34] was also preferred to use the term "heat-index" but gave the formula

$$M_b = M_v - H.I. - \Delta m_r + 0.9 \qquad (6)$$

for calculating absolute bolometric magnitudes, where H.I. and Δm_r have the same meanings as in equation (5). A number of 0.9 is added to equation (6) to make the zero-point of BC scales equal between Eddington [10], [30], and [34]. Note that, it is very obvious in (6) that H.I is equal to minus BC according to the definition of [26]. It is also same for equation (5) because the term $+\Delta m_r$ cancels first, then since H.I.= M_v - m_r, the term m_r also cancels then equation (5) could be written as $m_b = M_v$ - H.I. which also indicate H.I is equal to minus BC. It is clear in the paragraphs and tables of [30], [34] and others using H.I .that the H.I . is used for calibrating stellar temperatures, which was obvious in the comment of [34] "Heat-index like color-index is also zero for F5-G5 stars". That is, heat-index was used like color-index to indicate the effective temperatures of stars.

2.3. Surpassing definitions and the end of the pre-science period

At last, [26] preferred not to use the names previously existing as "luminous efficiency" nor "heat-index" but invented a new name "bolometric correction" (BC) also for calibrating the stellar temperature scale. Since BC is defined as M_{bol} – M_v or m_{bol} - V or as in the integral form given in equation (3) and because $M_{bol} = M_v + BC$ or $m_{bol} = V + BC$ or, that is, BC appears to be as a correction term to the visual (or photovisual) magnitudes, [26] preferred naming BC as bolometric correction. Despite its problems stated by [36], which were called paradigms by [13,15], this newest concept of BC has been used throughout the century and even today. The period after Kuiper [26] should be considered the normal science period that occurred first time in the development line (brief history) of BC (Figure 1) according to [27].

According to Eddington [10], the temperature scale set by spectral types was not certain. Consequently, one of the other purposes of Eddington was to improve
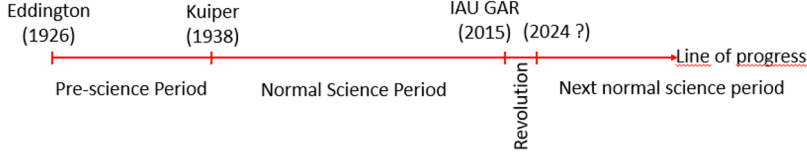
Fig. 1. Progress line of bolometric correction (BC) according to Kuhnian development of science.

the stellar temperature scale as well. He saw the potential of Table 1 for setting stellar temperatures. Since the radiation per unit area is proportional to T_e^4, he assumed the surface brightness (J) of a star is proportional to pT_e^4, where the parameter p is listed in the second column of Table 1. Thus, he expressed the surface brightness of stars in magnitudes as J=cons.-log $T_e+\Delta m$, where Δm is visual minus bolometric given in column 3. Nevertheless, Eddington was confused by assuming stars are like black bodies. For him, there were two effective temperatures. One comes from the Wien's law, Eddington named it T'_e (today T'_e is known as color temperature). The other is according to the Stefan-Boltzmann law, $L = 4\pi R^2 \sigma T^4$, called T_e. Eddington Commented *"For the Sun T'_e is about 4 per cent higher than T_e (approximately 6000° against 5740) and the same ratio may be expected to hold for all stars"*. The dilemma of two effective temperatures has been solved by Kuiper [26] who defined effective temperature only through the Stefan-Boltzmann law.

Expressing it in solar units as

$$L = R^2 (\frac{T_e}{T_{e,\odot}})^4 \tag{7}$$

Kuiper claimed, that since L is never known directly from observation, but usually only the absolute visual (or photovisual) magnitude, the above equation can be used in obtaining T_e only if a table of bolometric corrections is available. He means if R is available from the light curve solutions of eclipsing binaries, then the L of the stars with R, could be obtained from M_v as

$$M_{bol} = M_V + BC \tag{8}$$

$$M_{bol} - M_{bol,\odot} = 2.5 log \frac{L}{L_\odot}. \tag{9}$$

With known, L, R and $T_{e,\odot}$, the effective temperature of the star could be calculated by equation (7). That is, according to [26], tables of BC should be produced mainly for calibrating stellar effective temperatures. Because BC appears to be a

missing quantity or a correction term, equation (8) inspired Kuiper for the new name "bolometric correction" for the quantities M_{bol} - M_v = m_{bol} - V. The term "bolometric correction" was approved by others, thus the pre-science period, in which during many different hypotheses compete, ended for the line of progress (Figure 1), and the first normal science period started with the three paradigms: 1) BC of a star must always be negative, 2) Bolometric magnitude of a star ought to be brighter than its V magnitude, 3) The zero point of BC scale is arbitrary.

The origin of the first paradigm goes as far back as Eddington's comment: "At any other temperature P will be smaller and the star will be brighter bolometrically than visually". It is obvious in the definition of BC "M_{bol} - M_V = m_{bol} - V", BC becomes negative if $M_{bol} < M_v$ or $m_{bol} < V$, therefore, the origin of the second paradigm is the first paradigm.

Early BC producers were aware that BC values produced by different authors must agree with each other. Thus, they felt free to add a constant number, like 0.9 in equation (6), for consistency. This practice, however, later developed to be the third paradigm. Some may think that the integral form of BC, as in equation 3, requires an arbitrary constant because there are two integrals in the definition. This cannot be true because the definite integrals are written without constant. Only, indefinite integrals are written with a constant of integration.

2.4. Usages of BC in the normal science period before IAU GAR 2015

Although the concept of bolometric correction had been devised as an auxiliary parameter to be used primarily in the calibrations of stellar effective temperatures ([10], [26]), it was actively used in two more astrophysical applications: 1) for estimating masses and luminosities of single stars, 2) Double-checking or estimating parallaxes of double stars at least until the break caused by [2] occurred on the line of development of MLR [16] at the times when reliable observations of eclipsing binaries were limited, that is, before the quality and the quantity of the reliable solutions of detached double-lined eclipsing binaries (DDEB) giving accurate M and R within a few percent levels were used by [2]. Former was the only method in these years to obtain masses of singe stars at which Kepler's third law cannot be applicable. If a single star has a measured parallax or a distance (d), then its absolute visual magnitude M_v could be computed from an apparent magnitude by Pogson's relation

$$V - M_V = 5 log d - 5 \qquad (10)$$

assuming that the interstellar extinction does not exist or is corrected. Then, equation (8) was used to get M_{bol} from M_v and BC_V. For Eddington, M_{bol} was sufficient to get both the mass (M) and luminosity (L) of the star. However,

the general application was to use equation (9) to get L and then use the main-sequence classical MLR to get M from L.

The second application was also very useful because it is possible to obtain absolute orbital parameters and the masses of both stars through Kepler's third law if the distance of the double star is known. During these years, parallax measurements were not very accurate, it was possible to double-check the parallax of a double star. The sequence of the steps was as follows: 1) use classical MLR to obtain L of the each star from their masses., 2) Use equation (9) or use Eddington's MLR to get M_{bol} of the stars. 3) Use equation (8) and the BC of stars to get their absolute visual magnitudes (M_v). 4) Use equation (10) to confirm computed distances with the measured or estimated parallax ($\pi=1/d$) of the double star. Thus, double stars (visual binaries) and detached double-lined eclipsing binaries (DDEB) provided the most accurate stellar masses as accurate as observational errors permit.

3. RESOLUTION: IAU 2015 GAR B2

Arbitrariness attributed to the zero-point of various BC scales was one of the primary issues discussed by earlier IAU commissions. Previously, two of its commissions agreed on the zero-point of the bolometric magnitude scale by adopting a value for $M_{bol,\odot} = 4.75$ mag at the Kyoto meeting of 1997 ([3], pp. 141 and 181). On one occasion, the bolometric magnitude scale was set by defining a star with $M_{bol} = 0.00$ mag for an absolute radiative luminosity L=3.055x10^{28} W (see also [7]). At last the final resolution has been agreed in the IAU general assembly meeting in 2015 hereafter called IAU 2015 GAR B2.

The zero-point of the absolute bolometric magnitude scale was set according to

$$M_{bol} = -2.5logL + C_{bol} \tag{11}$$

with a statement "a radiation source with absolute bolometric magnitude M_{bol}= 0 has a radiative luminosity of exactly L_0=3.0128x10^{28} W and the absolute bolometric magnitude M_{bol} for a source of luminosity L (in W) is M_{bol} = -2.5 log (L/L$_0$) = -2.5 log L+71.197 425... That is, the zero-point constant for absolute bolometric magnitudes is C_{bol}=71.197 425... if L is in SI units, and C_{bol}=88.697 425... if L is in cgs units. Since nominal solar luminosity (L$_\odot$) is announced to be 3.828x10^{26} W in IAU 2015 GAR B2, using this value in equation (11), one can obtain $M_{bol,\odot} = 4.739$ 996 mag., which could be approximated as $M_{bol,\odot} \sim 4.74$ mag., for the absolute bolometric magnitude for the Sun.

The zero-point constant of the apparent bolometric magnitudes cannot be independent of the L_0 = 3.0128 x 10^{28} W chosen for setting absolute bolometric magnitude M_{bol} = 0 for a star at the distance, d, which produces a heat flux of

$$f_0 = \frac{L_0}{4\pi d^2} \tag{12}$$

just above the Earth's atmosphere if interstellar extinction does not exist or is negligible. Therefore, IAU 2015 GAR B2 defined the zero point of the apparent bolometric magnitude scale by specifying that m_{bol} = 0 mag corresponds to an irradiance or heat flux density of f_0= 2.518 021 002 ... x 10^{-8} W m^{-2} and hence the apparent bolometric magnitude m_{bol} for an irradiance f (in W m^{-2}) is m_{bol} = -2.5 log (f/f_0) = -2.5 log f -18.997 351... In another saying, equation (11) is adopted for the apparent bolometric magnitudes as

$$m_{bol} = -2.5 log f + c_{bol} \tag{13}$$

which scales irradiance (energy received from a star in a unit area just above the atmosphere) of stars rather than luminosities of stars thus the zero-point constant is c_{bol}= -18.997 351... if f is in SI units. Because the standard distance is 10 parsecs, one can obtain the value of f_0 from L_0 by dividing it into the surface area of a sphere with a radius equal to the distance (d) of 10 pc. One must be careful using the same type of units both L_0 (W) and d (meter). Since nominal solar irradiance ($f_\odot$) is 1361 W m-2, using this value in equation (13), one can obtain $m_{bol,\odot}$ = -26.832 mag for the apparent bolometric magnitude for the Sun.

3.1. Resolution and the paradigms

3.1.1. Resolution and paradigm one

Equation (11) could be adopted for the absolute visual magnitudes similarly as

$$M_V = -2.5 log L_V + C_V \tag{14}$$

where C_V would be the zero-point constant for the absolute visual magnitudes and L_V could be called the part of the luminosity falling into the window of the visual filter. Equation (11) could also be generalized for any band (ξ) of any photometric system as M_ξ = -2.5 log L_ξ+C_ξ. Consequently, the classical definition of BC (equation 1) of Kuiper implies that

$$BC_V = M_{bol} - M_V = 2.5 log \frac{L_V}{L} + (C_{bol} - C_V) \tag{15}$$

15

where the rightmost end of the equation (15) is obtained simply by subtracting equation (14) from equation (11).

Similarly, if equation (13) is re-arranged for the apparent visual magnitudes such as

$$V = -2.5 log f_V + c_V \qquad (16)$$

where c_V is the zero-point constant for the apparent visual magnitudes and f_V is the part of the total flux (f) falling into the window of the visual filter. Equation (13) could also be generalized for any band (ξ) of any photometric system as $\xi =$ -2.5log $L_\xi + c_\xi$. Consequently, the classical definition of BC (equation 1) of Kuiper involving apparent magnitudes would imply that

$$BC_V = m_{bol} - V = 2.5 log \frac{f_V}{f} + (c_{bol} - c_V) \qquad (17)$$

where the part of the equation (17) after the second equal sign could be obtained similarly by subtracting equation (16) from equation (13).

Remembering that the integral form of BC_V (equation 3) is equivalent to equation (17) here, equations (3), (15) and (17) could be combined for expressing the BC of the visual filter as

$$BC_V = 2.5 log \frac{L_V}{L} + (C_{bol} - C_V) = 2.5 log \frac{f_V}{f} + (c_{bol} - c_V)$$
$$= 2.5 log (\int_0^\infty S_\lambda(V) f_\lambda d\lambda / \int_0^\infty f_\lambda d\lambda) + C_2. \qquad (18)$$

This equation is more meaningful now after IAU 1015 GAR B2, where the value of C_{bol} and c_{bol} both were fixed up to the seventh digit in the magnitude scales. Using relative photometry, that is, comparing only similar kinds of magnitudes such as $V_1-V_1 =$ -2.5 log ([f_1 (V))/f_2 (V)], astronomers do not need to know the value C_V nor c_V because both cancel out automatically. Nevertheless, this does not change the fact both C_V and c_V are definite constants like C_{bol} and c_{bol}. Otherwise, astronomical photometry would not work.

Furthermore, because $f = \int_0^\infty f_\lambda d\lambda$ and $f_v = 2.5 log(\int_0^\infty S_\lambda(V) f_\lambda d\lambda)$, equation (1) certifies that the constant C_2 was claimed arbitrary constant of integration since it is seen after the two integrals in equation (3). Apparently, It is not a constant of integration because a definite integral never takes a constant. Secondly, it is not an arbitrary number but a definite number, which is equal to $c_{bol} - c_V$, since both c_{bol} and c_V are constants with definite values. In another saying, C_2 is not an arbitrary constant, but a required constant as indicated by equation (18). Only if one subtracts the two magnitudes of the same kind, he/she does not net to

know the value of the zero point constant because it cancels automatically, Otherwise, when subtracting two different kinds of magnitudes for a star, the zero-point constants do not cancel, thus treating this subtraction like subtracting the two visual magnitudes, or like two bolometric magnitudes, is a serious error. Because of this error of fallacy, that is, ignoring the zero-point constants of M_{bol} and M_v in the original definition of BC according to Kuiper, the paradigm 1 emerged.

Because the bolometric flux received from the star above the Earth's atmosphere f is proportional to the surface flux of the star σT^4, that is, $L = 4\pi R^2 \sigma T^4 = 4\pi d^2 f$, where f is the total flux at the d parsec away from the surface of the star, equation (18) implies also $(C_{bol}\text{-}C_V) = (c_{bol}\text{-}c_V)$. Thus, from equation (18) we can conclude that $C_2 = (C_{bol}\text{-}C_V) = (c_{bol}\text{-}c_V)$. Consequently we can also write:

$$BC_V - C_2 = 2.5log\frac{L_V}{L} = 2.5log\frac{f_V}{f} = 2.5log(\int_0^\infty S_\lambda(V)f_\lambda d\lambda / \int_0^\infty f_\lambda d\lambda). \quad (19)$$

which could be generalized for any band (ξ) of any photometric system as

$$BC_\xi - C_2(\xi) = 2.5log\frac{L_\xi}{L} = 2.5log\frac{f_\xi}{f} = 2.5log(\int_0^\infty S_\lambda(\xi)f_\lambda d\lambda / \int_0^\infty f_\lambda d\lambda). \quad (20)$$

Equation (19) clearly declares that it is not a bolometric correction in the visual band, but visual bolometric correction minus the zero-point of BC_V are always negative. On the other hand, equation (20) indicates that It is not the bolometric correction itself, but the bolometric correction minus the zero-point constant of the BC scale is always negative. This is because L_ξ/L, f_ξ/f and $(\int_0^\infty S_\lambda(\xi)f_\lambda d\lambda)/(\int_0^\infty f_\lambda d\lambda)$ are numbers between zero and one since $0<L_\xi<L$ and $0<f_\xi<f$. Logarithm of a number, which is between zero and one is always negative. Therefore, IAU 2015 GAR B2 literally cancels the paradigm 1: "BC of a star must always be negative" or one can say paradigm 1 must be corrected to indicate "BC of a star minus the zero-point constant of the BC scale is always negative"

Now, let us remember that the BC producers were divided into two schools; the school one assumed BC < 0 (paradigm one) for all stars, but the school two ignored this paradigm, that is, for the second school, not all stars but some limited number of stars might have a positive BC. Let us also remember, according to the original definition of BC = M_{bol} - M_v by Kuiper, if the zero-point constants of M_{bol} and M_v are assumed to be zero or totally ignored, one can write:

$$BC_V = M_{bol} - M_V = 2.5log\frac{L_V}{L} \qquad (21)$$

This equation could then be re-arranged for L as

$$L = L_V 10^{BC/2.5} \qquad (22)$$

Therefore, according to school one, BC > 0 is not possible, because if BC > 0, equation (22) implies L_V > L, which is unphysical. Only if BC < 0 would produce a valid L_V which is L_V < L. However, IAU 2015 GAR B2 indicate that equation (22) is not valid. The valid equation would be deduced from equation (20) as:

$$L = L_\xi 10^{(BC_\xi - C_2(\xi))/2.5} \qquad (23)$$

Considering equation (11) and (14) for a star with $M_{bol} = 0$ and $M_v = 0$, one can also deduce that the zero point constants (both C_{bol} and C_V) are positive and $C_{bol} > C_V$. Knowing that $C_2 = (C_{bol} - C_V) = (c_{bol} - c_V)$, one can conclude that the constant C_2 is a positive number. This fact, however, implies that all of the BC_V values, which are less than C_2, are valid to produce a physical L_V according to equation (23). Ignoring zero-points as in equation (22) is not permitted because every magnitude scale must have a zero point, and energy distribution of A0 V star (Vega in practice) is not constant but changes according to wavelength (or frequences), thus any kind of magnitude scale has its own zero-point, which are artificially set the intrinsic colors such as U–B, B–V, V–R like Johnson colors are zero for Vega. Despite the fact that zero-points of intrinsic colors are zero for Vega, each of the photometric bands (difference of magnitudes) have their own zero points, which are not equal to each other. Otherwise, Vega would have a constant intensity at all wavelengths, which is not the case. The school one, who assume BC < 0 always, are obviously in error. That is, it is possible for a star to have a BC which is positive according to equation (23). That means, equations (21) and (22) are not valid anymore after IAU 2015 GAR B2. In another saying, paradigm one is ruled out by IAU 2015 GAR B2.

3.2. Resolution and paradigm two

Influenced by the paradigm one, the followers of school one deduced the paradigm two from the first. An error occurred after previous error. That is, the followers of school one ignored the zero points constants of M_{bol} and M_v as in equation (21), thus, erroneous equation (22) was deduced, where only negative BC would produce a meaningful L, otherwise, if BC > 0, L_V becomes greater than L, which is unphysical. Consequently, the phrase "Bolometric magnitude of a star ought to be brighter than its V magnitude" became paradigm two. This statement is a kind of statement that, even if there is only one star with a positive BC (which could be in any band of any photometric system), the statement "Bolometric magnitude of a star ought to be brighter than its V magnitude" would be

abolished. Since paradigm one was shown to be abolished in the previous section, indicating that a BC value which is between zero and C_2 is possible according to equation (23), paradigms one and two were abolished together after IAU 2015 GAR B2.

3.2.1. Resolution and paradigm three

According to [15], IAU 2015 GAR B2 is a revolutionary document because it solves the problems related to the three paradigms, that is, it has a full potential to resolve the dilemma between the two schools [9, 21, 22, 26, 28, 29, 31, 37] obeying and [5, 6, 9, 12, 17, 18, 23, 24, 35] disobeying the paradigms. First of all, it replaces equation (9) with equation (11) and establishes a direct relation between M_{bol} of a star and its L. This cancels out the complexities caused by choosing different $M_{bol,\odot}$ by different authors. This means the arbitrariness problem (paradigm three) attributed to both the BC and the bolometric magnitude scales were demolished. It is very clear that according to equations (11) and (13), the zero-point constants of both absolute and apparent bolometric magnitude scales are definite values. Infinite accuracy of the constants intended (see three dots) by convention (decided in the IAU general assembly), but an accuracy up to the seventh digit after decimal point in the magnitude scale was certified. Thus, transferring L values to M_{bol} or vice versa, and transferring irradiance measurements into m_{bol}, or vice versa could be done very accurately, that is, the error contributions of the zero-point constants are practically zero. The Classical definition of BC_V according to Kuiper could be generalized for any band of any photometric system as:

$$BC_\xi = M_{bol} - M_\xi = m_{bol} - \xi \tag{24}$$

Although the zero point constants of bolometric and filtered magnitudes do not appear in the above equation, according to IAU 2015 GAR B2 and principles of photometry neglecting or canceling the zero points of bolometric and filtered magnitude scales are definitely wrong. According to IAU 2015 GAR B2 and principles of photometry, bolometric correction of the filtered magnitude (BC_ξ) has a definite zero-point constant as:

$$C_2(\xi) = C_{bol} - C_\xi = c_{bol} - c_\xi \tag{25}$$

The above two equations tell us that specifying the bolometric corrections only to the visual band would be wrong. There must be many different kinds of bolometric correction scales as many as the total number of bands in various photometric systems. Consequently, equation (25) indicates that each bolometric

correction scale has its own zero-point constant with a definite value specified to the band only. Considering the fact that there would be the unknown number of Bolometric correction scales, it would be meaningless for IAU to attempt fixing the unknown number of zero-point constants one by one. IAU 2015 GAR preferred the most logical way to fix the zero-point constant of the bolometric magnitude scale only. Fixing the zero-point of the bolometric magnitude scale ended up fixing the zero points of all bolometric corrections scales [13, 15].

4. NEW DEFINITIONS AND USAGES

With the same defining formula originally given for the visual magnitudes in equation (1) by Kuiper, which could also be generalized to any band of any photometric system, the verbal definition of BC must change. Equation (24) could be expressed as "BC of a star is the difference between its bolometric and one of its filtered magnitudes without ignoring both of the zero point-constants associated with the bolometric and the filtered quantities, unlike the other colors operating in relative scales such as U–B, B–V, V–R etc., which were set zero for a hypothetical A0V star artificially." One of the two main purposes of IAU 2015 GAR B2 was standardizing the bolometric magnitude scale accurately and repeatably for transforming photometric measurements into radiative luminosities and irradiances, independently of the variable Sun. Unfortunately, this revolutionary document was ignored or unnoticed [1, 6, 15] so its revolutionary potential was noticed about five years later by [12], who was trying to convince the referees that arbitrariness attributed to the zero-point of the BC scale is a paradigm demolished by IAU 2015 GAR B2 during the refereeing stage of newly determined bolometric corrections from DDEB stars in the solar neighbourhood. Unfortunately, [12] was forced to remove everything else other than newly determined BC_V values. Removed arguments were rearranged and improved later by [13], where the standard bolometric corrections were defined as the following: if a bolometric magnitude of a star is determined from its observed radius (R) and effective temperature (T_{eff}) to give L= $4\pi R^2 \sigma T^4$, then if one plugs this L to equation (11) to get M_{bol} and at last calculates BC_ξ of any band by $BC_\xi = M_{bol}$ - M_ξ, where M_ξ should be corrected for atmospheric and interstellar extinctions, then the obtained BC_ξ is a standard BC.

The luminosity of a star is not a directly observable parameter. While discussing the three methods and their accuracies providing L of a star from its observed quantities, [14] defined the standard luminosities later. If the L of a star is computed from its observed R and T_{eff}, it is standard by definition. Thus, this direct method relying on the Stefan-Boltzmann law was the only method to have standard luminosities, while other methods using the mass-luminosity law,

and bolometric corrections providing stellar luminosities were not considered even reliable before IAU 2015 GAR B2. Thus, standard L was defined as: if the luminosity of a star is calculated from its M_{bol} using equation (11), where M_{bol} is from the relation $M_{bol} = M_{\xi} + BC_{\xi}$ using a standard BC, it is called a standard luminosity [14]. According to [14] a single band standard luminosity from a standard bolometric correction and absolute magnitude could have an accuracy about 10 per cent, that is, both methods, one using the Stefan-Boltzmann law and the other using a standard BC, are comparable. A method of improving standard stellar luminosities with multiband standard bolometric corrections was suggested recently by [4]. Multiband standard BC and BC – T_{eff} relations in the forms of fourth-degree polynomials were calibrated independently from the parameters of 209 DDEB binaries with main-sequence components. Standard L of 406 main-sequence stars with most accurate parameters were calculated by the two methods. The method one is the classical direct method with the Stafan-Boltzmann law. The method two used absolute magnitudes and standard bolometric corrections at Johnson B, V, and Gaia EDR3 G, G_{BP}, G_{RP}, filters. Curves of the standard BC – T_{eff} relations of [4] at five photometric bands are displayed in Figure 2.
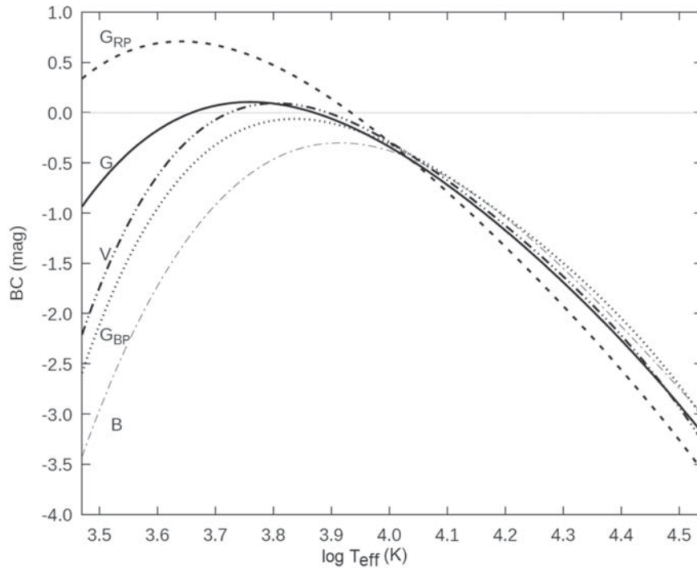
Fig. 2. Independent BC-T_{eff} relations at Gaia G, G_{BP}, G_{RP} and Johnson B,V [4]

A single-band standard BC – T_{eff} relation is expressed in the form of a fourth-degree polynomial as

$$BC = a + bX + cX^2 + dX^3 + eX^4 \qquad (26)$$

**Table 2.** Coefficients of multiband BC-log T_{eff} relations taken from [4].

Coeff.	BC_B	BC_V	BC_G	$BC_{G_{BP}}$	$BC_{G_{RP}}$
a	1272.43	3767.98	1407.14	3421.55	1415.67
	±394.2	±288.8	±256.7	±293.6	±253.3
b	1075.85	3595.86	1305.08	3248.19	1342.38
	±394.4	±290.9	±258.9	±296.1	±255.4
c	337.831	1286.59	453.605	1156.82	475.827
	±147.7	±109.6	±97.67	±111.7	±96.34
d	46.8074	204.764	70.2338	183.372	74.9702
	±24.53	±18.32	±16.34	±18.68	±16.12
e	2.42862	12.2469	4.1047	10.9305	−4.44923
	±1.552	±1.146	±1.023	±1.169	±1.009
N	402	402	402	342	386
rms	0.136257	0.120071	0.11068	0.126577	0.109179
R^2	0.9616	0.9789	0.9793	0.9738	0.9884

where a, b, c, d, e are coefficients of a fourth-degree polynomial with a variable X = log T_{eff} . One needs to know the effective temperature of the star to calculate its multiband BC using empirically determined coefficients in Table 2. The number of stars used in the calibration (N), standard deviation (SD), and correlation coefficient (R^2) are also given in the table.

Knowing that, observations (apparent magnitudes), and BC - T_{eff} relations of each band are independent, at last, one obtains five independent L using independent multiband bolometric corrections. One can improve the accuracy of L by taking the average of the independently predicted L values. [4] preferred not to take the average of this L but to use independently predicted M_{bol} values of each band to calculate mean M_{bol} and its standard error first. Then, one could use equation (11) to calculate corresponding L and its uncertainty from the mean M_{bol} and its uncertainty. The mean M_{bol} was calculated by [4] as:

$$M_{bol} = \frac{1}{N}\Sigma_i^n M_{bol,i} \tag{27}$$

Where $M_{(bol,i)} = M_i + BC_i$, bolometric magnitude of the star at each band i = B, V, G, G_{BP}, and G_{RP}. n is the number of photometric bands having an available standard BC. It is clear in equation (27) that by increasing the number of bands (n), one can improve the accuracy of M_{bol} and consequently the accuracy of L could be improved.
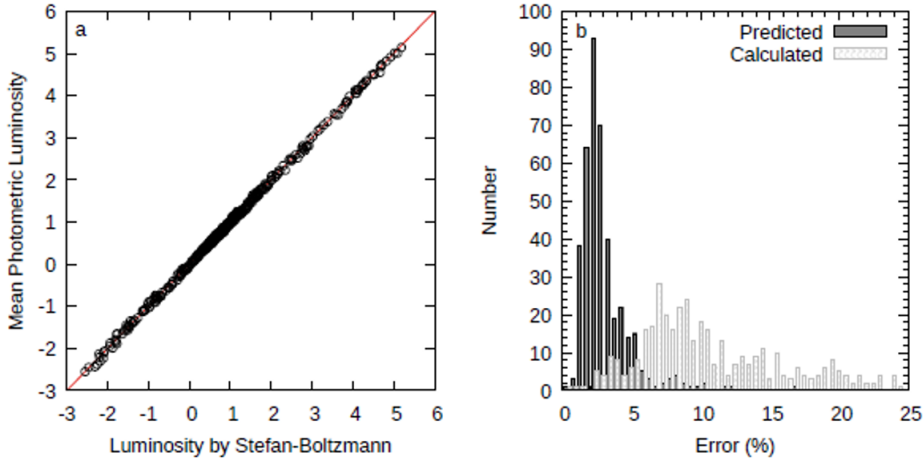
Fig. 3. a) Comparing predicted (from photometry) and calculated (from R and T_{eff}) L of the sample main-sequence stars. b) Histogram distributions of the errors associated with predicted (dark) L is compared to the histogram distributions of errors associated with calculated (gray) L. ([4])

Being limited to five photometric bands, [4] succeeded to obtain very accurate stellar luminosities, even more, accurate luminosities than the direct method could provide as displayed in Figure 3 where the left box shows a very high correlation ($R^2 = 0.9999$) between the predicted luminosities involving multiband (B, V, G, G_{BP} and G_{RP}) standard bolometric corrections and calculated luminosities from the direct method using observed R and T_{eff} according to the Stefan-Boltzmann law. Because of IAU 2015 GAR B2 and standardization it caused, first time in the history of astrophysics, there is a new method providing standard stellar luminosities, which could be three or four times more accurate than the luminosities from the direct method with Stefan-Boltzmann law.

[11] tested multiband BC and BC – T_{eff} relations by recovering luminosities of DDEB stars from which the standard multiband BC and BC - T_{eff} relations were calibrated. [11] added one more band, TESS, into the list and increased the number of bands having standard BC to six and then tested the six-band standard BC - T_{eff} relations by recovering the luminosities (L) and observed radii (R) of the most accurate 241 single host stars (281 Main-sequence, 40 subgiants, 19 giants and one-pre-main-sequence) successfully from their apparent magnitudes, Gaia DR3 parallaxes and standard BC at six-bans B, V, G, G_{BP}, G_{RP} and TESS. The main-sequence standard BC and BC-T_{eff} were found useful not only in recovering L and R of the main-sequence stars but also in other luminosity classes such as giants and subgiants.

5. CONCLUSIONS

- With the same defining formula first suggested by Kuiper, $BC_\xi = M_{bol} - M_\xi = m_{bol} - \xi$, the old verbal definition of BC, used in the first normal science period, must change to:

  BC of a star is the difference between its bolometric and one of its filtered (pass band) magnitudes without ignoring both of the zero-point constants associated with bolometric and filtered quantities in absolute scale, unlike the other colors operating in relative scale (U–B=B–V=V–R=...=0 of A0V star), which were set to be zero artificially for a hypothetical star A0V.

- The zero-point constants of BC scales are as many as the number of pass-bands. C_2 (ξ)=C_{bol}- C_ξ=c_{bol}- c_ξ, where ξ could be one of the passbands of various photometric systems and capital C imply absolute, while small c for apparent, magnitude scales.

- The Zero-point constant of a BC scale is not arbitrary. It is a definite number in magnitude scale unique to the passband.

- It is not the BC of a star but BC – C_2 is always negative, where C_2 is the zero-point constant of the BC scale in question.

- The Zero-point constant (C_2) of a BC scale could be a positive number (See Figure 2). This means all BC < C_2 for a photometric band are valid, that is, bolometric magnitudes (M_{bol} or m_{bol}) of some stars could be dimmer than their filtered magnitudes (M_ξ, ξ). This, however, does not mean the part of the luminosity corresponding to M_ξ is greater than the total luminosity. This is because L_ξ=L $x10^{(BC_\xi - C_2(\xi))/2.5}$ is valid to produce L_ξ< L for all photometric bands.

- The normal science period (Figure 1) was ended in 2015 in the year when IAU 2015 GAR 2 issued and the silent revolution [15] has been started because all of the problems associated with the three paradigms (1) BC of a star must always be negative, 2) Bolometric magnitude of a star ought to be brighter than its V magnitude, 3) The zero point of BC scale is arbitrary) were shown to be resolved.

- The new normal science period will start after the new definition of BC and the consequences itemized above are digested among contemporary astrophysicists.

REFERENCES

1. Andrae R., Fouesneau M., Creevey O., et al., 2018, A&A, **616**, A8

2. Andersen J., 1991, A&ARv, **3**, 91

3. Andersen J., 1999, Proc. Twenty-Third Gen. Assem., Transactions of the IAU, XXIIIB. Kluwer, Dordrecht

4. Bakış V., & Eker Z., 2022, AcA, **72**, 195

5. Bessell M.S., Castelli F., Plez B., 1998, A&A, **333**, 231

6. Casagrande L., Vanden Berg D.A., 2018, MNRAS, **475**, 5023

7. Cayrel R., 2002, Lejeune T., Fernandes J., eds., ASP Conf. Ser. Astron. Soc. Pac., San Francisco, CA, **274**, 133

8. Code A.D., Bless R.C., Davis J., Brown R.H., 1976, ApJ, **203**, 417

9. Cox A.N., 2000,eds., Allen's Astrophysical Quantities, ISBN:0387987460. AIP Press, Springer, New York

10. Eddington A.S., 1926, in The İnternal Constitution of the Stars, Cambridge University Press, Cambridge, UK

11. Eker Z., Bakış V., 2023, MNRAS, **523**, 2440

12. Eker Z., Soydugan F., Bilir S., et al., 2020, MNRAS, **496**, 3887

13. Eker Z., Bakış V., Soydugan F., & Bilir S., 2021a, MNRAS, **503**, 4231

14. Eker Z., Soydugan F., Bakış V., & Bilir S., 2021b, MNRAS, **507**, 3583

15. Eker Z., Soyducan F., Bakış V., Bilir S. & Steeer I., 2022, AJ, **164**, 189

16. Eker Z., Soydugan F., Bilir S., 2024, Phy. Astron. Rep., **2**, 41

17. Flower P.J., 1977, A&A, **54**, 31

18. Flower P.J., 1996, ApJ, **469**, 355

19. Hertzsprung E., 1911, Pub. Astrop. Obser. in Potsdam., 1, **22**, 63

20. Hertzsprung E., 1923, Bull. Astron. Inst. Netherlands, **2**, 15

21. Habets G.M.H.J., Heintze J.R.W., 1981, A&AS, **46**, 193

22. Hayes D.S., 1978, Proc. Symp., Washington, D.C., November 2-5, 1977. Dordrecht: Reidel, 76

23. Johnson H.L., 1964, BOTT, **3**, 305

24. Johnson H.L., 1966, AR A&A, **4**, 193

25. Johnson H.L., & Morgan W.W., 1953, ApJ., **117**, 313

26. Kuiper G.P., 1938, ApJ., **88**, 429

27. Kuhn T.S., 1962, The Structure of Scientific Revolutions

28. McDonald J.K., & Underhill A.B., 1952, ApJ **115**, 577

29. Pecaut M.J., Mamajek E.E., 2013, ApJS, **208**, 22

30. Pettit E., Nicholson S.B., 1928, ApJ, **68**, 279

31. Popper D.M., 1959, ApJ, **129**, 647.

32. Russell H.N., 1914, Pop. Astron. **22**: 275

33. Russell H.N., Adams W.S., Joy A.H., 1923, PASP, **35**, 189

34. Strömberg G., 1932, ApJ, **75**, 115

35. Sung H., Lim B., Bessell M.S., Kim J.S., Hur H., Chun M., Park B., 2013, JKAS, **46**, 103

36. Torres G., 2010, AJ, **140**, 1058

37. Wildey R.L., 1963, Nature, **199**, 988

$^)$

VARIABILITY OF Hα LINE IN SUPERGIANT STARS OF SPECTRAL TYPE B, A AND F

A. B. Hasanova [a*], *A. M. Khalilov* [a]

[a] *Shamakhy Astrophysical Observatory named after N.Tusi of Ministry of Science and Education of the Republic of Azerbaijan, Shamakhy, Azerbaijan*

The variability in the profiles of the Hα line profiles in selected B, A and F spectral class supergiant stars was comparatively analyzed based on the spectra obtained at the 2-meter telescope at the Shamakhy Astrophysical Observatory. This study investigates the variability in the values of the parameters characterizing the profiles of the Hα line and the changes in profile shapes in the spectra of the supergiant stars HD 190603 (B1.5 Ia), HD 208501 (B8 Ib), HD 187982 (A2 Ia), HD 207260 (A2 Iae), HD 195593 (F5 Ib), HD 163506 (F2 Ibe) and HD7927 (F0 Ia). For each star, the reasons for these changes were investigated, leading to general conclusions.

From the study of the selected supergiant stars of spectral type B, A and F, it can be concluded that from the supergiant stars of spectral type B to the supergiant stars of spectral type A and F, i.e., as the effective temperature decreases, the variability in the atmosphere of the star is observed less. In particular, stellar wind is stronger in B spectral type supergiant stars. Some of the ejected matter disperses into the interstellar medium, some returns and falls on the surface of the star, and some collects around the star, and turns into a disk or inhomogeneous cover. In F spectral type supergiant stars, since the temperature is relatively low, the magnitude of the variability in the star atmosphere is small. Therefore, in the studied F-type stars, the profile of the Ha line is often observed as a full absorption profile.

Keywords: supergiant stars – Hα line profile – spectral variability.

1. INTRODUCTION

Supergiant stars are variable stars with an extended envelope and a sparse, non-stationary atmosphere. According to the modern theory of evolution, hydrogen has already burned out in the core of such stars, and the process of burning

---

Table 1. Some information about the program stars.

№	Catalog number	Name of the star	Spectal class	Effective temperature T_{eff} , K	Apparent magnitude	Observation period
1	HD 190603		B1.5 Ia	19500	$5^m.65$	2010÷2019
2	HD 208501	13 Cep	B8 Ib	13000	$5^m.80$	2013÷2019
3	HD 187982		A1, A2 Iab	9300	$5^m.57$	2016÷2019
4	HD 207260	v Cep	A2 Iae	9200	$4^m.29$	2015÷2019
5	HD 7927	φ Cas	F0 Ia	7300	$4^m.98$	1986-2018
6	HD 195593	44 Cyg	F5 Iab	6100	$6^m.2$	2004-2014
7	HD 163506	89 Her	F2 Ibe	6000	$5^m.46$	1975÷2017

helium and heavier elements has begun. Due to the large mass of these stars, their evolution process is fast, their lifetime is short, they are considered young stars and they are mainly located in the Galactic plane. Their age can be about 30÷100 million years, and they are most often observed in active regions - open star clusters, the spiral arms of the Galaxy and irregular galaxies. In random cases, they are observed in the core of spiral galaxies, globular star clusters, and elliptical galaxies. Due to their brightness, these stars are widely used in studying the distribution of chemical elements at long distances from the Sun, as well as within the Galaxy. Therefore, the study of supergiant stars in order to determine the spiral structure, shape and size of our Galaxy, as well as other galaxies, is one of the most pressing issues of modern astrophysics.

In this work, the variability of the Hα line profile in the spectra of B, A, and F spectral class supergiant stars was analyzed comparatively based on the spectra obtained from the 2-meter telescope of the Shamakhy Astrophysical Observatory named after N.Tusi of the Ministry of Science and Education of the Republic of Azerbaijan. The variability in various stars belonging to the mentioned spectral classes has been studied by us as well as by other authors. Table 1. provides the lists of the stars studied in this work and the values of their various parameters.

2. OBSERVATIONAL MATERIAL AND ITS PROCESSING

Spectral observations of the program stars were obtained using CCD camera installed in Universal Astro Grid Spectrograph (UAGS) with an echelle-spectrometer at the Cassegrain focus of the 2-meter telescope at the Shamakhy Astrophysical Observatory named after N.Tusi. Until 2016, the spectra were obtained with a 530×580 pixel CCD camera, providing a spectral resolution of

R = 14000. The observation materials cover the spectral range $\lambda 3960 - 6600$. Detailed information about the characteristic and working principle of this camera is given in Mikayilov [19]. Since 2016, spectra were obtained using a 4000×4000 pixel CCD camera at the Cassegrain focus, with resolutions of R = 28000 and R = 56000. The dispersion curve was constructed using the spectrum of the daytime sky. Two or three spectra of the star were obtained in a single night. Since there was no strong variation in the spectrum of the star during the night, the spectra were averaged. The spectra were processed using the DECH-20 and DECH $-$ 20 T software packages presented by [6]. The error in measuring the equivalent width is less than 5%. The error in measuring the radial velocity is not greater than 2 km/s. Observational materials and their processing methodology are described in detail in our previous works Khalilov [18].

3. VARIABILITY IN SUPERGIANT STARS OF SPECTRAL CLASS B

The changes in the values of the parameters characterizing the Hα line profiles in the spectra of supergiant stars HD 190603 and HD 208501, typical representatives of B spectral class supergiant stars, as well as the variations in the shape of the profiles, have been extensively studied in our previous works.

The apparent magnitude of the supergiant star HD190603=HR 7678 varies in the range of $5.56 \div 5.70$, it is a blue supergiant star with a spectral class B1.5 Ia [2]. Its absolute stellar magnitude $M_v = -7.5$. In the Galactic coordinate system, its galactic longitude is l=69°.5, the galactic latitude is $b = +0°.4$ [15] and the distance to the star is1961.5 pc [5].

It was shown in [14], that the Hα line profile consists of weak absorption and emission components on the violet side and is observed in the form of clearly distinguishable P Cygni type profiles. It was found that the emission component of the profile consists of one, two, and sometimes three components (Figure 1 (a)).

It has been proved that the radial velocity and equivalent width of the absorption and emission components of the Hα line change with a period of about 100 - 120 days according to time. These variations have been explained by the pulsation of the stellar atmosphere.

The supergiant star **13Cep = HD208501 = HR8371** is a supergiant star that is included in the group of eruptive (flammable, erupting) stars with an irregular change in brightness with apperent magnitude V = 5.80, spectral type B 8 Ib . Its brightness varies from 5.935 to 5.865. Its absolute stellar magnitude $M_V = -4.25$. In the Galactic coordinate system, the galactic longitude is l = 100°.39, the galactic latitude is b = +1°.68. The distance to the star is 700 pc [21].

In our article mentioned in [17], it was shown that in the spectrum of the supergiant star HD 208501, the shape, structure and the value of the spectral parameters characterizing the profile of the Hα line profile show greater variability. The Hα line profile is observed in the following forms depending on the activity of the star (Figure 1 (b)): a) full absorption profile;

b) normal P Cygni-type profile: absorption and on the red wing emission component;

c) inverse P Cygni-type profile: absorption and on the violet wing emission component;

d) weak emission component on both wings and absorption profile in the center;

e) full emission profile;

f) attenuation of the intensity of the absorption and emission components to the level of the continuous spectrum.

In our previous works [17], it was found that the radial velocity and equivalent width of the Hα line profile change within a week or even shorter intervals. As a result of the study of the Balmer series of hydrogen and the lines of various elements in the spectrum of the star HD 208501, and as a result of the calculations, it was shown that the radial velocities of the elements whose lines are observed in the star's atmosphere are stratified by layers. It was determined that the amplitude and average value of the changes of radial velocities of the lines increase from the lower to the upper layers of the atmosphere.

These observational results prove the existence of a rotating, non-homogeneous density disk-like gaseous envelope around the star HD 208501 directed at a certain angle towards the observer, these changes are explained by the pulsation of the star and the interaction between the star and its circumstellar envelope Khalilov et al., [17].

As can be seen, in the spectrum of both stars, a P Cygni-type profile was observed in the Hα line (Figure 1 (a, b)). It is known that the appearance of the P Cygni-type profile in the spectrum proves the presence of an expanding gaseous envelope around the star and a strong matter loss.

It should be noted that the formation of a P Cygni-type profile can be considered characteristic in hot supergiant stars with a wide envelope. Such profiles, which are mainly observed in the Hα line profile, are sometimes also observed in the HeI and HeII lines. In the spectrum of the supergiant star HD 190603 which has a higher effective temperature, a P Cygni-type profile is clearly observed in the Hα, Hβ and helium lines profiles. In the supergiant star HD 208501, whose effective temperature is 6500K lower than that of the supergiant star HD 190603, P Cygni- type profile is only observed in the Hα line profile. Thus, the decrease in effective temperature directly affects the spectral variability of the star. The vari-

ability of the mentioned stars is explained by the result of interaction between the envelope surrounding them and the stellar atmosphere. By studying the various spectral lines observed in the spectrum and their parameters, it is possible to explore the interaction mechanism between stellar atmosphere and the surrounding envelope.
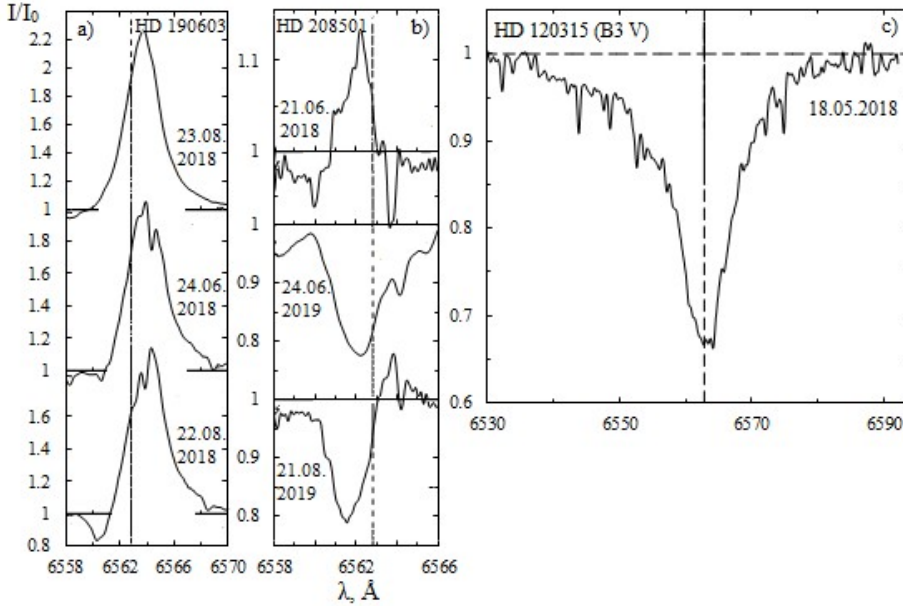
Fig. 1. Profile of the Hα line in the spectrum of stars HD 190603 (a) and HD 208501 (b). On the right, for comparison the spectrum of the Hα line in the spectrum of a standard star HD 120315 (c), of spectral class B.

4. VARIABILITY IN SUPERGIANT STARS OF SPECTRAL CLASS A

Supergiant stars of spectral class A, have a lower effective temperature compared to supergiant stars of spectral class B. From the perspective of spectral variability, they are slightly different stars. In this work, the change in the values of the parameters characterizing the profiles of the Hα line and the shape of the profile in the spectrum of the stars HD 187982 and HD 207260, which are typical representatives of these stars, were comparatively studied.

The supergiant star HD 187982 HR 7573 has an apparent magnitude of V = 5.57, according to [3], and a spectral class of A1-A2 Iab. The HD 187982 supergiant star is the brightest star of the Vul OB4 star cluster. The HD187982 supergiant is the brightest star in the Vul OB4 star cluster. In the Galactic

coordinate system, the galactic longitude is $1 = 61°.89$, the galactic latitude is $b = -1°.04$, and the distance to the star is 1095.77 pc [4].

In our previous work [13], time-dependent changes in spectral parameters and shape of profiles of Hα and other lines of the Balmer series were studied based on observations of the supergiant star HD 187982 in 2016-2018.

It has been shown that the profile of the Hα line changes over time with a quasi-period of 25-29 days [13].
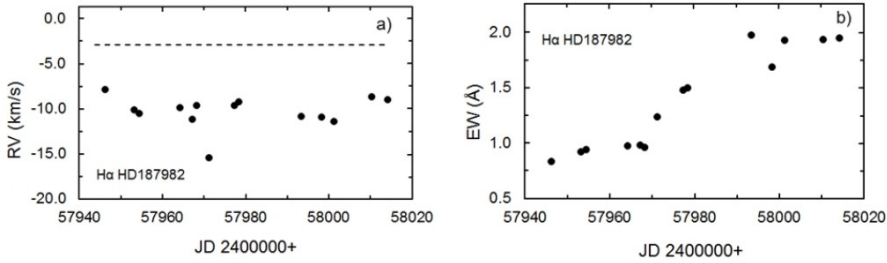
Fig. 2. (a). Radial velocity variations of the Hα line in 2017. For the date JD 2457971.340 a displacement with an amplitude of $\sim$7 km/s is observed. The dashed line indicates the velocity of mass center of the star. (b). Time variations of equivalent widths EW of the absorption line Hα in 2017

As can be seen from Figure 2 (a), on the date JD 2457971.340, a sudden shift of the Hα line to the violet side with a velocity of -12 km/s relative to the velocity of the mass center of the star, was detected, and then return to its initial position. On the same date, an increase in the equivalent width of the line was also observed, and this increase gradually continued until the end of the observation season, Figure 2 (b). Simultaneously with these events on the indicated date, until the end of the observation season, the strengthening of the emission components of the Hα line was observed, Figure 3 (a). These changes indicate that the stellar wind spreading in the stellar atmosphere is not stable and occurs in the form of mass ejections from the surface of the star. This leads to an increase in the amount of atoms contributing to the radiation lines and the equivalent width of those lines. The increase in the intensity of the emission components in the violet and red wings of the line indicates that the ejected mass is collected in the stellar environment and a part of it slowly disperses into the interstellar medium over time, while another part collects around the star, forming a gas disk, and a certain portion falls back onto the surface of the star.
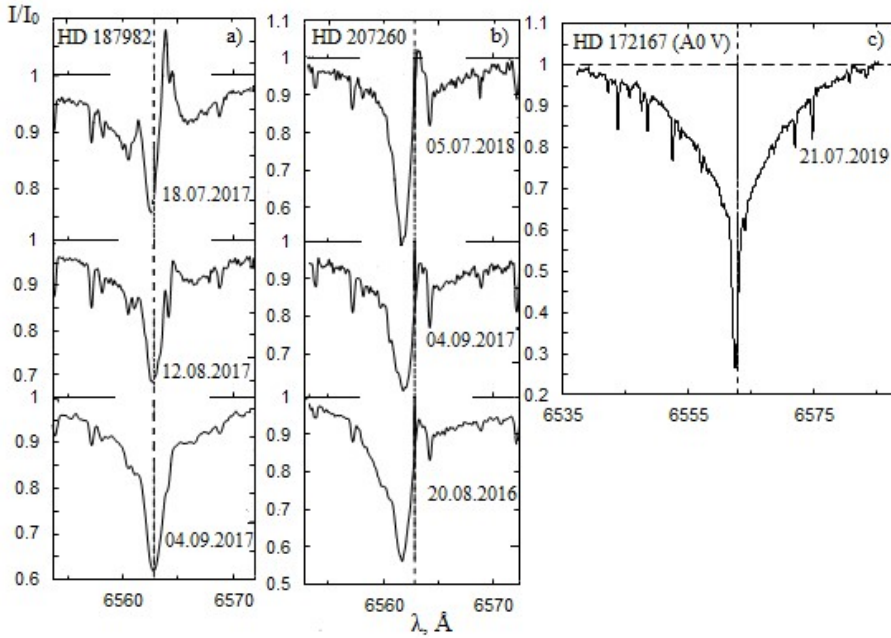
Fig. 3. Examples of the Hα line profile in the spectra of the stars HD 187982(a),
HD 207260(b) and standard HD 172167(c).

The apparent magnitude of the supergiant star **vCep = HD207260 = HR8334**
is V = 4.29 [3], the spectral class is A2 Ia. [8]. In the Galactic coordinate system,
the galactic longitude is l = 102°.3, the galactic latitude is b = +5°.93 [21], the
distance to the star is 2083 pc [26].

In [11], based on the comparative study of the emission and absorption com-
ponents of the Hα line profiles observed on the basis of 25 spectra of the star
HD 207260 in 2016 2019 , it was found that the value of the spectral parameters
characterizing the shape, structure and profile of the Hα line profile exhibit vari-
ability. The Hα line profile is observed in the form of a full absorption profile and
a normal P Cygni-type profile, figure 3 (b). As a result of the calculations, it was
determined that the radial velocity of the absorption and emission components of
the Hα line, as well as the equivalent width of the absorption component, varies
with a quasi-period of 35-40 days. An increase in the absolute value of the radial
velocity in the absorption component of the Hα line is observed with a decrease
in the value equivalent width and that of the emission component. That is, this
event occurs synchronously. Researches show that this variation occurs as a result
of the pulsation of the star and the interaction between the stellar atmosphere
and the circumstellar envelope.

Figure 3 presents the profile of the Hα line in the spectra of the supergiant stars HD 187982 (A1-A2 Iab), HD 207260 (A2 Iae) and the standard star HD 172167 = αLyr (A0 Va) of spectral class A. It is clearly seen from the profiles that in the standard star αLyr, the Hα line profile is observed in the form of a smooth full absorption profile. In supergiant stars, however, the Hα line profile is observed in various forms, including inverse and normal P Cygni types. The reason for the P Cygni-type profile is the result of the presence of an expanding gas envelope around the star, or the ejection of matter in the form of a strong stellar wind as in the case of B spectral type supergiant stars.

As seen, the shape and spectral parameters of the Hα line profile in the spectra of supergiant stars of spectral class A vary with time. However, since the effective temperature of these stars is relatively low, their variability scale is also smaller compared to that in B spectral class supergiant stars. Despite the fact that the Hα line is observed in the form of a P Cygni-type profile in the spectra of supergiant stars of spectral class A, the profile of the Hα line does not weaken to the level of a continuous spectrum in these stars. At the same time, P Cygni-type profile is not observed in other lines of the Balmer series of Hydrogen and in the Helium line formed in deeper layers.

5. VARIABILITY IN SUPERGIANT STARS OF SPECTRAL CLASS F

Supergiant stars of spectral class F have lower effective temperatures than supergiant stars of spectral class B and A.

The study of the F spectral class stars HD 7927 and HD 195593, along with the star HD 163506 located at high latitudes, is of significant importance for evolutionary theory. For this reason, this work presents a comparative analysis of the values of the parameters characterizing the profiles of the Hα line in the spectra of these stars and the changes in their profiles. The work primarily utilizes results mentioned in published articles based on research conducted in previous years.

The star φ Cas HD 7927 = HR 382 is one of the brightest hypergiant stars in our Galaxy. Spectral class is F0 Ia, apparent magnitude is $V = 4.98$ [25]. In Galactic coordinate system, the galactic longitude is $l = 127°$, the galactic latitude is $b = -4°$ [22]. The star is located at a distance of z = -150pc from the Galactic plane. The yellow hypergiant star φCas is a member of the NGC 457 open star cluster.

In [12], the spectral study of this star has been discussed. As a result of the research, it was found that there were no significant changes in the Hα line profiles and values of the equivalent width in the spectrum of the φCas star. No asymmetry has been observed in the Hα line profiles, proving the presence of the stellar wind and mass loss. However, variations in the radial velocity of the Hα

and H$_\beta$ lines over time have been detected. In the H$_\beta$ line, it has been determined that the value of the radial velocity defined according to the center of the profile is lower than the radial velocity according to the half-width of the line. This proves that the velocity of the stellar wind decreases in the upper layers of the atmosphere where these lines effectively form. Based on the results of the calculations conducted, the authors explained time-dependent variation of the equivalent width and radial velocity in the Hα, H$_\beta$, Hγ, and etc. by the pulsation of the star.

The star 44 Cyg=HD 195593 = HR7847 has an apparent magnitude of $V = 6.2$, a spectral class of F5 Iab, and a galactic latitude of $b = -1°.4$, a galactic longitude of $l = 76°.4$. The star is located at a distance of z $= -34$pc from the Galactic plane [22].

In [10], the spectral study of the star HD 195593 is discussed. The profiles of the Hα, H$_\beta$, Hγ and H$_\delta$ lines observed in the spectrum of the star have been constructed, the value of the parameters characterizing these lines: the equivalent width (W$_\lambda$), the line depth (R$_\lambda$) and the halfwidth of the line ($\Delta\lambda$(R/2)) have been calculated. It has been shown that, as in star HD 7927, the Hα line profile in the spectrum of the supergiant star HD 195593 does not change its shape significantly over time and is observed only in the form of a full absorbtion profile. However, the radial velocity of the Hα line changes depending on time.

Among A and F spectral type stars, particularly significant are the post-AGB type stars located at high galactic latitudes. These stars are of great importance from the point of view of evolution, because according to evolutionary theory, supergiant stars should be young and massive, but according to the same theory, young and massive stars should be located close to the Galactic plane [1], for the first time in 1951, observed the existence of A and F type supergiant stars located at latitudes of 22° or higher far from the Galactic plane. Despite over 70 years having passed, the evolutionary stages of such stars have not yet been clearly explained. There are several hypotheses about the evolution of high-latitude supergiant stars:

1) A group of young, massive stars formed in the Galactic plane, later left the Galactic plane and moved away;

2) A group of old, low-mass stars with high luminosity at the end of evolution;

3) Stars formed through the evolution of binary systems.

Most of the results obtained from the observation prove the truth of the second hypothesis. The observation of A and F type supergiant stars in some old globular star clusters far away from the Galactic plane has already become the focus of many scientists. Note that such supergiants are sometimes called post-AGB (Asymptotic Giant Branch) stars.

Post-AGB stars are luminous objects of low to intermediate initial mass ($M_* \leq 8 - 9M_\odot$) in the final stage of evolution: they have completed their

Asymptotic Giant Branch (AGB) evolution with a period of intense mass loss $\left(10^{-7} - 10^{-4}M_{\odot}yr^{-1}\right)$. These stars evolve rapidly toward hotter effective temperatures while maintaining roughly constant luminosity, but they are not yet hot enough to ionize the circumstellar material and emerge as a Planetary Nebula (PN), before eventually cooling down to become a white dwarf (WD).

Post-AGB stars cover a wide range of effective temperatures, from extreme AGB stars just after the superwind [9], to objects like AFGL 618, which are on the verge of inonizing the circumstellar matter. The star HD 163506, which is a representative of this type of star, has been studied in this work.

The star 89 Her = V441 = HD 163506 (spectral class F2 Ibe, V = 5.46 mag) behaves like a pulsating variable star and is the strongest example of a UU Her type star [24].

It is located at a galactic latitude of b $= 23°19'$ and a longitude of l $= 51°43'$ [20], at a distance of z $= 2.2$kpc from the Galactic plane. [16] presents the following results.

The Hα line contains one, two, or three absorption components, while the emission component is consistently observed in the red wing of the Hα line. The third most blue shifted component was observed by Sargent and Osmer [23] on July 17, 1962, and by the authors on August 26, 1975 with maximum radial velocities of -150 km/s and -180 km/s, respectively. The radial velocity of the first absorption component of the Hα line for these dates is several times lower and equals -10 km/s and -55 km/s, respectively. It can also be seen from Table 1. that the velocity of the emission component of the Hα line changes significantly. The radial velocity varies from $+56$ km/s on July 17, 1982 [16], to $+12$ km/s on August 26, 1975. The obtained spectra of the supergiant 89 Her of the Hα absorption line in the period 1955-2017, showed that the three components were observed only twice, on July 17, 1962 and August 26, 1975. The remaining observations indicate that the absorption profiles of the Hα line contain only one or two components. For the study, we focused exclusively on only the second component. At the same time, the values of the radial velocity of the emission component vary from $+60$ km/s for on April 30, 1966 [23] to $+7$ km/s on July 10, 2010. Figs. 3 and 4 illustrate, on the basis of the spectra obtained by us between 2000 and 2017, and by Gangi et al. [7] between 1993 and 2018, the changes over time in the values of the radial velocities Vr and terminal velocity of the Hα absorption component V$^{\infty}$, and simultaneously, the equivalent widths W . It can be seen that the radial velocities, terminal velocity, and equivalent widths exhibit periodic changes with a period of approximately P $= 5000$ d. The studies have shown that, in addition to the short-period variations found earlier by various researchers, there are also long-period variations in the atmosphere of this star. It has been found that the radial velocity and equivalent width of the NaI D absorption line vary with a pe-

riod of approximately 5000 days. This is interpreted as the motion of the binary system 89 Her around an invisible component. The orbital elements of the system were determined within the model of a spectral-binary system with a period of 5000 days. In figure 4, the Hα line profiles in the spectra of the F spectral class
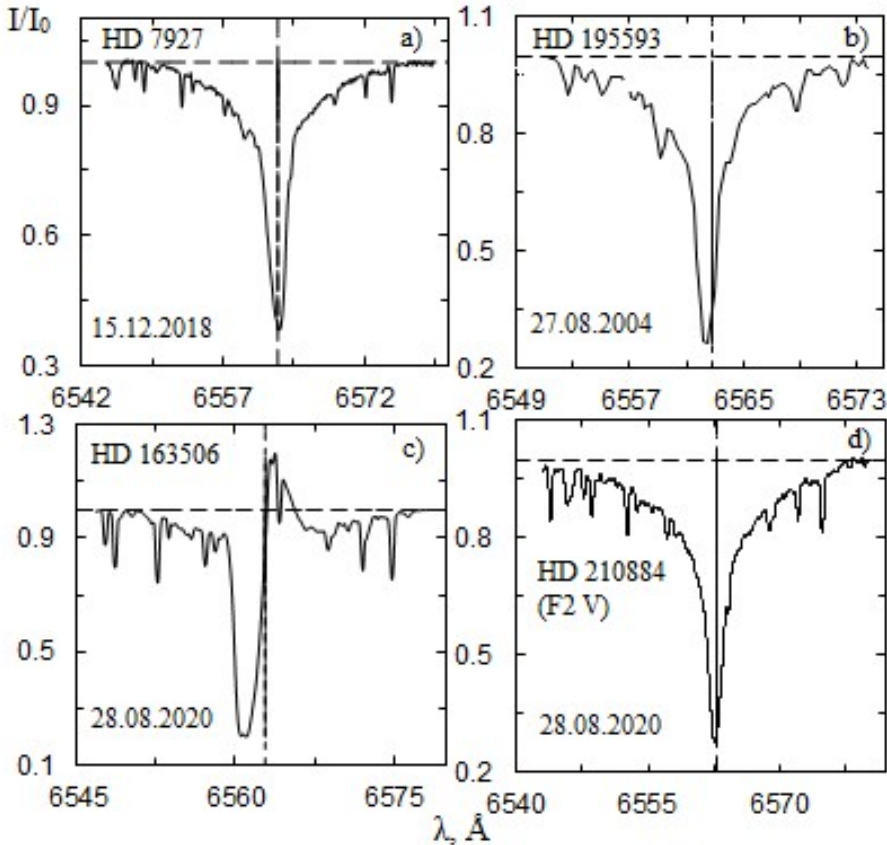
Fig. 4. Examples of the Hα line profile in the spectra of stars HD 195593(b), HD 7927(a), HD 163506(c) and the standard star HD 210884(d).

supergiant stars HD 7927 (F0 Ia) and HD 195593 (F5 Iab), the high-latitude Post AGB star HD 163506 (F2 Ibe), and the standard star HD 210884 (F2 V) are presented. It is clear from the examples that Hα line profile is observed in the form of a smooth full absorption profile in supergiant stars of spectral class F and in the main sequence star. In contrast, a P Cygni-type profile is observed in the high latitude Post AGB star HD 163506.

Summary. Apparently, in the spectrum of supergiant stars of spectral class F, the shape of the Hα line profile does not change depending on time and is observed in the form of an absorption profile. However, radial velocity of the Hα

line varies with time. The fact that the profile of the Hα line is observed only in absorption indicates that the stellar wind in these stars is much weaker compared to B and A type stars. Therefore, as the effective temperature of a supergiant star decreases, the scale of variability in its atmosphere also decreases. Nevertheless, in the high-latitude F spectral class Post AGB star HD 163506, the H α line profile is observed in various forms, and is of the P Cygni-type. As a result of research, it became clear that this variability is related not to physical processes occurring within the star, but rather to the binarity of the star.

6. CONCLUSIONS

At the conclusion of the conducted research, the following results were obtained:

1. In B spectral class supergiant stars, the Hα line profile can be observed in the following forms depending on the phase of the activity of the star (Figure 1):

a) full absorption profile;

b) normal P Cygni-type profile: absorption and on the red wing emission component;

c) inverse P Cygni-type profile: absorption and on the violet wing emission component;

d) weak emission component on both wings and absorption profile in the center;

e) full emission profile;

f) attenuation of the intensity of the absorption and emission components to the level of the continuous spectrum.

It is characteristic for hot supergiants of spectral class B to have a surrounding extensive envelope or disk. The conducted studies indicate that the higher the effective temperature of the star, the greater the scale of variability.

2. In the spectra of the A spectral class supergiant stars, the form the Hα line and spectral parameters change over time. However, the scale of this variability is weaker compared to B spectral class stars. The conducted studies indicate that the Hα line profile in A spectral class supergiant stars is observed in the form of a P Cygni-type profile; however, the profile does not show a decline to a continuous spectral level in these stars.

3. In the spectra of F spectral class supergiant stars, the form of the Hα line profile does not change over time and is observed in the form of a full absorption profile. However, the radial velocity of the Hα line varies with time.

4. In the high-latitude F spectral class supergiant HD 163506, the Hα line profile is observed in the form of P Cygni-type. This is explained by the fact

that the star being in its final evolutionary stage, that is, in the post-AGB stage. The 5000-days periodic variability in the profile of the Hα line is explained by the binarity of the star.

5. Our investigations have revealed that in the studied stars, from B spectral class supergiant stars to A and F spectral slass supergiant stars, which corresponds to a decrease in the effective temperature, the variability observed in the Hα line profile in the spectrum becomes less pronounced (excluding the case of the binarity of the star).

Also, as a result of non-stationary processes occurring in the stellar atmosphere with a decrease in the effective temperature of the star: the stellar wind, the loss of matter weakens, variability is less observed.

REFERENCES

1. Bidelman W.P., 1951, ApJ, **113**, 304

2. Clark J.S., Najarro F., Negueruela I., et al., 2012, A&A, **541**, 36

3. Ducati J.R., 2002, CDS/ADC Coll. Electron. Catalogues, **II/237**,0

4. Gaia Collaboration, 2020, CDS/ADC Coll. Electron. Catalogues, **I/350**,0

5. Gaia Collaboration, 2020, VizieR On-line Data Catalog: I/350. A&A, **649**, A1

6. Galazutdinov G.A., 1992, Spets. Astrofiz. Obs. Ross. Akad. Nauk, Preprint, **92**,14

7. Gangi M., Giarrusso M., Munari M., et al., 2021, MNRAS, **500**, 926

8. Gray R.O., Garrison R.F., 1987, ApJS, **65**, 581

9. Habing H.J., van der Veen W., Geballe T., 1987, in Late Stages of Stellar Evolution, ed. Kwok S., Pottasch S. R., Dordrecht, D. Reidel, 91

10. Hajiyeva G.M., 2019, News ANAS, Ser. Phys.-Tech. Math. Sci., Phys. Astron., **39**, 88

11. Hajiyeva G.M., Khalilov A.M., Hasanova A.B., 2023, News ANAS, Ser. Phys.-Tech. Math. Sci., Phys. Astron., **43**, 124

12. Hasanova A.R., Khalilov A.M., Hajiyeva G.M., Adigozelzade H.N., 2015, AzAJ, **10**, 35

13. Hasanova A.B., Baloglanov A.Sh., Ismailov N.Z., 2021, AzAJ, **16**, 44

14. Hasanova A.B., Khalilov A.M., 2022, AzAJ, **17**, 128

15. Hobbs L.M., 1985, ApJ, **298**, 357

16. Khalilov A.M., Hajiyeva G.M., Hasanova A.R., Hasanova A.B., 2022, AcA, **72**, 297

17. Khalilov A.M., Hasanova A.B., Samedov Z.A., et al., 2021, News ANAS, Ser. Phys.- Tech. Math. Sci., Phys. Astron., **41**, 167

18. Khalilov A.M. & Hasanova A.R., 2007, Az.AJ, **2**, 20

19. Mikayilov Kh.M., Khalilov V.M., Alekberov I.A., 2005, Circular of the Shamakhy Astrophysical Observatory, **109**

20. Molina R.E., 2012, Rev. Mex. Astron. Astrofis., **48**, 95

21. Pan K., Federman S.R., Cunha K., et al., 2004, ApJS, **151**, 313

22. Rufener F., 1976, A&AS, **26**, 275

23. Sargent W., Osmer P.S., 1969, in Mass Loss from Stars, Proc. 2nd Trieste Colloq. Astrophys., 57

24. Sasselov D.D., 1984, Ap&SS, **102**, 161

25. Stencel R.E., Pesce J.E., Bauer W.H., 1989, AJ, **97**, 1120

26. Van Leeuwen F., 2007, A&A, 474, 653

)

OBSERVATIONS OF NEUTRON STAR MERGER REMNANTS AS PART OF THE GRANDMA COLLABORATION

Sh. A. Agayeva [a], *Z. Vidadi* [a], *N. Z. Ismailov* [a], *S. Antier* [b*]

[a] *Shamakhy Astrophysical Observatory named after N.Tusi of Ministry of Science and Education of the Republic of Azerbaijan, Shamakhy, Azerbaijan*

[b] *Université Côte d'Azur, Observatoire de la Côte d'Azur,CNRS, Artemis, Boulevard de l'Observatoire, 06304 Nice, France*

This article summarizes the key findings and methodologies of the GRANDMA (Global Rapid Advanced Network Devoted to the Multi-messenger Addicts) collaboration in observing the remnants of neutron star mergers. To achieve this, the Côte d'Azur Observatory in France, the Shamakhy Astrophysical Observatory in Azerbaijan, and their collaborators have pooled their observational efforts, astrophysical analyses, and expertise within an international consortium known as GRANDMA. The GRANDMA collaboration is a global network of observatories dedicated to the rapid follow-up of gravitational wave events and other transient astronomical phenomena. The primary objective of the GRANDMA collaboration is to detect and characterize the electromagnetic counterparts of gravitational wave events, particularly those originating from neutron star mergers. Neutron star mergers are cataclysmic events that provide critical insights into a variety of astrophysical phenomena, including gravitational waves, heavy element nucleosynthesis, and the behavior of matter at nuclear densities. By employing a diverse array of telescopes across the globe, GRANDMA aims to provide rapid, coordinated observations that cover multiple wavelengths, from optical to radio. These observations are crucial for identifying kilonovae, the transient optical and infrared emissions powered by the radioactive decay of heavy elements synthesized during the merger.

Keywords: Neutron stars – gravitational waves – LIGO – VIRGO detectors

---

1. INTRODUCTION

Neutron stars are the remnants of stellar explosions that have been proposed over the course of decades. The likelihood of their merger being observed as gravitational wave signals instead of being directly seen as new and transient sources is very small. The first event in 2017 opened the era of multi-messenger astronomy. The prosperous era of multi-messenger astronomy opened up in 2017 with the observation of a binary neutron star merger, GW170817, in both gravitational waves (GW) and electromagnetic radiation domains. Being some of the most massive stellar remnants, we expect neutron stars to be found across the universe since they are long-lived objects as remnants of supernova explosions. Factors that affect population statistics in astronomical objects include a binary fraction with other compact objects. Part of the distribution of compact objects, i.e., white dwarfs and neutron stars, together along the Hubble time, can form white-dwarf neutron stars with a second common-envelope stage and the tidal disruption of a white dwarf by a neutron star. These were considered rare but have had an increased probability of occurring in the detector era and hence also in the future [7–13]. The influence on the local and cosmic landscapes by neutron star mergers happening in the present universe includes an observable gravitational wave signal and the possible production of r-process elements (especially the heaviest elements observed in the solar system, but abundances are spread over mass due to this form of nucleosynthesis). Emitted with the s-process nucleosynthesis signal of the normal immediate post-collapse environment, one event offers one possible method of distinguishing between these two production sites based on the observed s-process abundances in environments currently presenting process abundances from ejecta measurements of energetic objects associated with gravitational waves, like this kilonova as the source was named. This paper now presents the observations of the actual gravitational wave-neutron star merger afterward.

1.1. Background on Neutron Star Mergers

The coalescence of close binary neutron stars is expected to form many different phenomena, as the neutron star merger and the ejection driven by microphysical processes are determined by a large number of uncertain processes. The strong gravity of close binary systems causes stars to orbit each other about twice per second. If the orbit of these stars is influenced by the merger such that the stars interact when they are still many times larger than the distance between them, gravitational radiation dominates, leading to the merger of the neutron stars. In the particular case of binary neutron stars, lumps leaving the system

will typically form a torus, which will quickly collapse to form a single compact object that may be an unstable massive neutron star, a quark star, or a black hole. The currently known neutron stars are around two times the mass of the Sun and approximately 10 km in size. Their "rock solid" strength is determined by the strong nuclear forces, but when neutron stars are compacted in close binaries, they are only held by gravity, so the neutron stars slowly spin towards each other due to the emission of strong gravitational waves. During this collision, neutron star matter and surrounding plasma reach supranuclear densities, extreme gravitational acceleration, enormous pressures, and temperatures - eventually converting into black holes and the rest of the debris accreting and forming an accretion disk. The debris and the accretion disk re-radiate in optical/infrared or ultraviolet as well as in the X-ray and radio frequencies. Finally, a very massive magnetized ball of fire produced by collapse or black hole formation is born and creates a fireball - most of the events are expected to be accompanied by the production of gamma-ray bursts. Initially, during the infall, a weak shock wave is produced which keeps stalling to bounce back and makes the stellar surface explode-eventually spreading matter and radiating pressure into the high-density debris-producing the ultraviolet and optical/infrared light. This phenomenon is also known as kilonovae or macronovae. Thus, we expect neutron star mergers at two different tidal disruption rates to give rise to a weak kilonova and a strong kilonova, with the kilonova optical/infrared light being about 100 times brighter in the case of a strong disruption. The strongest explosions that make most of the heavy elements are powered by the remnants that achieve a high mass that becomes gravitationally unstable and converts into a black hole. Simulation results are yet to arrive. Ultimately, when the neutron stars merge at high speeds, the heavy elements in the part of the very tight binary zone are in fact overlapping electron clouds preventing the neutron stars from merging cleanly and ejecting an excess amount of heavy elements, creating the first epoch of cosmic heavy element formation. Neutron star mergers were predicted long ago, but observationally they were directly established with the detection of gravitational waves from a significant event. Before this event, many direct and indirect candidates for this event were searched without detections. This event was associated with a short gamma ray burst by gamma-ray satellites in an initially identified optical source at a redshift of about 0.01. A specific experiment was used to search for electromagnetic counterparts in the radio band from the short gamma-ray burst associated with this event. Subsequent searches for radio counterparts were conducted with various networks. Additionally, another array was also used, and there were no positive radio detections of the counterpart. A series of efforts were made to scan southern skies hoping to catch any radio jet from the event. Systems were analyzed, but again there were no successful detections. In the ten

weeks after the detection of the gravitational waves, many instruments worldwide detected the merger remnant in optical and X-ray bands.

1.2. Importance of studying neutron star merger remnants

Neutron star mergers are relevant for other types of astronomy as well. Gravitational wave astronomy can make a variety of inferences about cosmic populations and systems by comparing the distribution of events in such parameter spaces as masses, spins, and merger rates, but for most inferences astrophysical priors are necessary and can only be obtained from observations. Neutron star mergers also place important constraints on stellar evolution and galaxy population models, for instance by providing direct evidence of the existence of heavy element-rich black hole accretion disks, the prevalence of neutron star recycling, and the possible contribution from gravitational wave events in constraining the equation of state. As such, nuclear astrophysical and multi-messenger observations of kilonovae will be critical for the advancement of gravitational wave astronomy.

2. THE GRANDMA COLLABORATION

In this collaboration, the Côte d'Azur Observatory in France, the Shamakhy Observatory in Azerbaijan, and their partners have united their observational efforts, astrophysical analyses, and expertise within an international consortium known as GRANDMA. Now, in the gravitational wave era, people including the GRANDMA collaboration are working to understand the remnants that their composite signal makes apparent. For on-axis remnants, the initial bright transient evolves to form a kilonova, a blue/NIR signal that spans all times with a characteristic dimming between several days and weeks after the merger. It is now essential to bridge these observational gaps. During the LIGO/Virgo O3 run, GRANDMA included more than 300 astrophysicists from about 25 research institutes in countries such as France, Italy, United States, Ukraine, Azerbaijan, Georgia, Spain etc. More details on the composition of the collaboration, how it works, and a series of applications are described in a dedicated work. The GRANDMA collaboration has an agreement on sharing images, photometric position-time series, and derived model constraints of all detected counterparts. It is our aim to inform the community about active fallback remnants and transient events at a speed faster than that produced by a single survey and beyond the expected evolution of the detection pipelines. Further, the results presented here will soon feed into a combined analysis including gravitational wave data. In this paper, we detail the remnants studied and discovered using this observa-

Fig. 1. Location of the GRANDMA telescopes on the world map. Credit: J.-G. Ducoin, Follow-up of gamma-ray bursts with the GRANDMA network, GRB221009A and GRB230812B.

tional approach thus far.One staple of GRANDMA has been the combination of gravitational waves and subsequent electromagnetic data. GRANDMA combines multi-messenger facilities such as the LIGO and Virgo detectors, which observed GW190425, with optical and X-ray telescopes. Rapid-response, all-sky transients are often common between classes of electromagnetic follow-up. Such coordinate triangulation is currently implemented on a campaign basis by contractors, computed from their relative field of view, axes, and axes as outlined in the observation request. LIGO/Virgo and GRANDMA are prime examples of quickly disseminated transient alerts with public searchable records of collaborations initiated with exact timestamps [1–6].

In the GRANDMA collaboration, we have formed a worldwide consortium of research groups that are observing and theory communities, data analysis pipelines, and facilities to study neutron star merger remnants. These groups include individuals from various universities and research institutions, with additional network support and continuing discussions with other relevant researchers. The goal of GRANDMA is to support and strengthen investigations of the HEN, KN, GW optical-IR afterglow, and XR optical afterglow with electromagnetic and/or neutrino multi-messenger observations. GRANDMA observers bring a range of skills and strengths. This includes the expertise and facilities required for optical and IR observations of nearby galaxies and gamma-ray events made by a range of wavelength observatories, gravitational wave data analysis exper-

tise, and facilities to analyze gamma-ray and putative prompt kilonova emissions or other electromagnetic counterparts, plus state-of-the-art neutrino searches to provide high-quality multi-messenger follow-up data. Our aim within the observation community is to coordinate all such real-time triggered multi-messenger observations and data around the time of any GW signal detection, as well as to programmatically and routinely compare these signals and coordinate jointly published results at later times [1–6].

3. FUTURE PROSPECTS

What new techniques and data will be available in the near future to approach the study of these remnants? The first most notable improvement will derive from significantly better and more collaboratively secured low-latency GW localizations with the advent of the Vera Rubin Observatory, as demonstrated in our results and will be improved in the near future by the SVOM-MXT observatory. Following a joint US-German project which will highly refine the above estimates will soon after be launched. It now appears that the Maunakea Spectroscopic Explorer will enter its construction phase, thanks to cooperation. The combination of these two projects will be a major leap forward in observational capabilities as they provide joint GW and EM localizations, allowing for matched early spectra within a day of the merger.

Which new surveys and missions aimed at investigating the above science goals will become operational or begin their on-sky sampling in the coming years? As detailed in documentation on the timelines and survey capabilities, such joint localizations will become routine in the 2030s and beyond, as the number of events increases, if a collaboration were to be established. In the interim years, Vera Rubin and Maunakea-hosted data will remain possibly the best way for our community to first study with EM radiation these "new systems," as possibly discovered directly post-merger by neutron star neutrino emission and secondly search for r-process EM kilonovae and electromagnetic counterparts from IW echoes that emerge on timescales of seconds to days after merging.

4. DISCUSSION AND CONCLUSION:

The GRANDMA collaboration plays a critical role in the multi-messenger astronomy era by focusing on the rapid and coordinated observation of neutron star merger remnants. These events are not only associated with gravitational waves but also produce rich electromagnetic counterparts, such as kilonovae, which are

key to understanding the synthesis of heavy elements and the physics of compact object mergers.

We are still at the outset of the new era of multi-messenger neutron star merger research. The current investigations involving newly established collaborations or collaborations under heavy development and commissioning leverage the state-of-the-art in technology, instruments, and software capabilities, as well as the international scientific networking opportunities for making fantastic new discoveries and measurements in the first years of the new decade. Many new projects, including new or upcoming facilities and projects that we were unable to claim results on, are expected to release first conclusive findings in this period of the beginning of the new decade [14–16]. Even though EM signatures of these systems are faint and rare, the field is currently in the process of a significant advance. Electromagnetic follow-up can significantly improve the GW localization on the sky by up to several orders of magnitude, and currently several ongoing projects focus on transient discoveries associated with large-area, time-domain surveys. Some of the projects aim to train their telescopes on the area of the reported GW candidates as fast as possible after the alerts. In parallel, our understanding of such counterparts has improved, particularly thanks to developments in data analysis in the past years, and we are lucky to count on several new, exotic telescopes and surveys that are or will be looking for these peculiar systems from various perspectives.

REFERENCES

1. Antier S. et al., 2020, arXiv preprint, (arXiv:2008.03962)

2. Antier S. et al., 2022, Proc. SPIE, **12186**, 121861H

3. Barres de Almeida, U., 2021, preprint (arXiv:1907.08516)

4. Burns E., 2020, Living Rev. Relativ., **23**, 1

5. Filippenko A.V., 2020, in Origin and Evolution of the Universe: From Big Bang to Exobiology, **24**, 99

6. Gorkavyi N.N. & Tyul'bashev S.A., 2021, Astrophys. Bull.,**76**, 1

7. Howell S.B. et al., 2024,,Front. Astron. Space Sci., **11**, 1304616

8. Hussenot-Desenonges T. et al., 2024, MNRAS, **530**, 1

9. Ismailov N.Z., Antier S., Vidadi Z., Agayeva Sh., 2023, Proc. 74th Int. Astronaut. Congr.

10. Kann D.A. et al., 2023, ApJL, **948**, L12

11. Koliogiannis P.S. & Moustakidis, C.C., 2021, ApJ, **909**, 166

12. Lattimer J.M. & Prakash M., 2004, Science, **304**, 536

13. Marino A., 2020, The explosion of massive stars and their compact remnant, PhD th esis, 113

14. Molla M.C. & SNEWS Collaboration, J. Phys.: Conf. Ser., 2021, **2156**, 012001

15. Moskvitch K., 2020, Neutron stars: the quest to understand the zombies of the cosmos, 296

16. Pian E., 2021, Front. Astron. Space Sci., **8**, 645646

$^{)}$

RADIO EMISSION FROM LATE STAGE SUPERNOVA REMNANTS

A. I. Asvarov [a], *H. I. Novruzova* [a*]

[a] *Institute of Physics of Ministry of Science and Education of the Republic of Azerbaijan, Baku, Azerbaijan*

In this paper, we consider radio emission from supernova remnants in the late stages of evolution. It is expected that a significant part of the observed SNRs are in the late stages of evolution. It is shown that the model of radio emission based on the mechanism of diffusive shock acceleration (DSA) is able to explain the statistics of observed SNRs. The possibility of DSA operation and the occurrence of radio emission in SNRs at the radiative stage of evolution is discussed. It is shown that empirical $\Sigma - D$ dependencies are not suitable for determining distances to SNRs.

Keywords: Supernova Remnants -– Radiative SNRs —— Radio emission

1. INTRODUCTION

Radio emission is an important property of supernova remnants (SNRs). Although SNRs are now observed at almost all wavelengths of the electromagnetic spectrum, for galactic supernova remnants the most complete information is available in the radio range. The latest catalog of galactic supernova remnants contains 310 objects [4], the vast majority of which are nonthermal radio sources. It is generally accepted that the action of the mechanism of diffusive shock acceleration (DSA) at the front of the main shock wave is responsible for the generation of the relativistic electrons emitting synchrotron radio emission from supernova remnants. However, the injection problem – from what energies and what percentage of background particles are subject to acceleration – remains unresolved despite the mechanism's universality and physical clarity. It is possible to answer this problem and other questions concerning the physics of shock waves and space

plasma by using data on the radio emission of SNRs. At the same time, a realistic model of the evolution of radio emission can help clarify issues like how the ISM affects SNR life, how SNRs contribute to the formation of the ISM's structure, and what part of the galaxy SNRs occupy. The fact is that simple estimates show that the number of SNRs in the galaxy is no less than 2000. A natural question arises about where to look for these not yet discovered SNRs, what properties, including in the radio range, they have. To answer these questions, it is preferable to study supernova remnants at the middle and late stages of evolution. The majority of in-depth research on SNR radio emission focuses on young SNRs, where, depending on the kind of supernova, circumstellar matter plays a significant role. Currently, the richest observational material is available for young supernova remnants, and the most detailed physical models are built for them. However, the role of young remnants in the overall statistics of SNRs is insignificant because the expansion of the supernova remnant occurs with deceleration, resulting in a far larger number of old and extended remnants than young ones [5]. It is expected that among the observed SNRs, the majority are in late stages of evolution. Several factors make it easier to study evolved supernova remnants: the explosion energy is the determining characteristic of the supernova, regardless of the type of supernova or the mass of the ejected shell; the state of the plasma behind the shock wave front becomes more equilibrium; and the use of the diffusion acceleration mechanism in the approximation of test particles becomes justified. Factors that complicate the study of the SNR in the middle and late stages of evolution are taking into account of the pressure in the ISM and the consideration of the onset of the radiative phase and fundamental changes in the structure of the remnant.

2. EVOLUTION OF SUPERNOVA REMNANTS.

During its evolution, a supernova remnant goes through several stages or phases: the free expansion phase; the Sedov adiabatic phase and the post-adiabatic phases. In the first two stages, the total energy of the remnant is conserved. In the first stage, all the energy is in the form of the kinetic energy of the shell ejected during the explosion of the star, in the second stage $\simeq 70\%$ of the total energy is converted into thermal energy, the remaining 30% is in the form of the kinetic energy of the shock wave, more precisely, this division depends on the adiabatic index γ. For statistical calculations, the law of expansion of the outer shock wave in the first two stages can be described by a single equation

describing the conservation of the kinetic energy of the remnant shell:

$$\left(M_{ej} + \frac{4}{3}\pi\rho_0 R_s^3 \right) \cdot \left(\frac{dR_s}{dt} \right)^2 = 2E_{0k}, \tag{1}$$

which gives for the shock wave velocity $v_s = \frac{v_{0s}}{\sqrt{1+(R_s/R_0)^3}}$, where R_s is the outer radius of the shock wave, in other words the SNR radius, $R_0 = (3M_{ej}/4\pi\rho_0)^{1/3}$, and $v_0 = \sqrt{2E_{0k}/M_{ej}}$. From Eq.(1) it follows that when $R_s \ll R_0$ the velocity is constant $v_s = v_0 = \mathrm{const}$ (free expansion) and $v_s = v_{os} \cdot (R_s/R_0)^{-3/2}$ at $R_s >> R_0$ in accordance with the Sedov expansion law [3]:

$$R_s = \left(\frac{\xi E_0}{\rho_0} \right)^{1/5} t^{2/5} \tag{2}$$

where E_0 is total (thermal plus kinetic) energy of the blast wave, ξ is the dimensionless numerical constant, which depends on the adiabatic index of the plasma γ: $\xi = 2.026$ for $\gamma = 5/3$. Since an exact self-similar solution to the shock wave structure [9] is available, it is simple to perform an analytical examination of the physical processes in the SNR shells, making the phase of adiabatic expansion the most studied. At this phase, the SNR actively emits at almost all wavelengths of the electromagnetic spectrum. It should be noted that this phase does not account for ambient pressure. The end of the Sedov adiabatic phase occurs when this condition begins to be violated. The evolution of the SNR in this case will occur without large energy losses, but the structure of the shock wave ceases to be self-similar. In the work [4] presents an analytical model describing the SNR structure, considering the ambient pressure in the interstellar medium. The distinctive feature of the SNR development in this approximation is that the law of change of the forward shock wave's radius will differ from Sedov's law (2) only slightly, while the relative thickness of the shell will increase significantly compared to Sedov's solution (Fig 1).

The radiative cooling phase begins when the shock wave speed drops to ~ 200 km/s. During this phase, a thin cold shell, formed as a result of the rapid loss of thermal energy in the area behind the front of the forward shock wave, will expand in snowplow mode. The expansion law of this shell is determined by the pressure difference inside the shell and in the surrounding interstellar medium. Note that the forward shock wave continues to exist ahead of the dense shell, although its expansion rate decreases sharply due to the pressure drop behind the front. The simplest model describing the structure of the SNR in the radiative phase was proposed in the work [3], in particular, it was shown that the cooling region behind the front of the external shock wave has a locally self-similar structure. In the next section we will consider whether the conditions for DSA
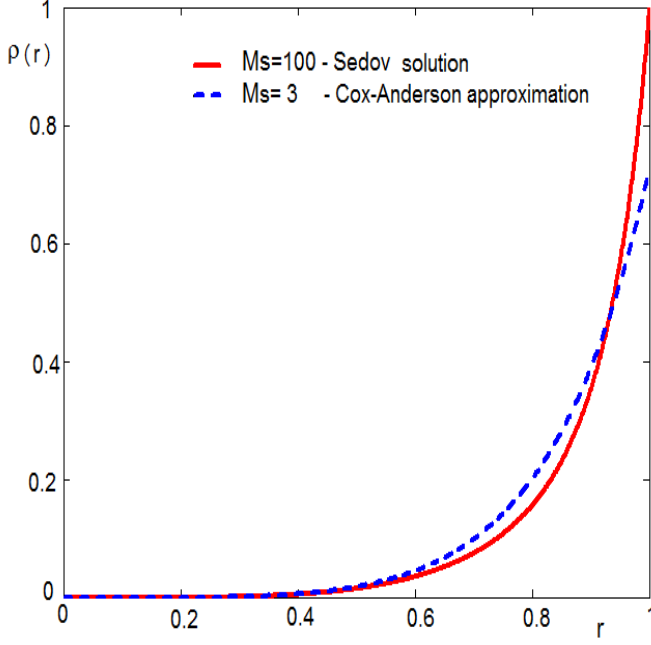
Fig. 1. Radial dependence of the normalized density of matter for Mach numbers Ms 100 and 3.

operation in this phase exist, since we are interested in the radio emission of the SNR.

3. RADIO EMISSION OF SNR

It is well known that radio emission of shell-type SNR has a synchrotron nature, i.e. relativistic electrons moving in magnetic fields are responsible for the radio emission.

The power-law dependence of the flux of observed radio emission on frequency in the form $S_\nu \propto \nu^{-\alpha}$ indicates that the radio-emitting electrons are distributed in energy according to the power law

$$N_e dE = K_e E^{-q} dE, \tag{3}$$

and the spectral index of radio emission α is directly related to the spectrum index q by the relation

$$\alpha = \frac{q-1}{2} \tag{4}$$

Isotropically distributed electrons with the distribution function (3) in the magnetic field B radiate synchrotron radio emission with the coefficient

$$\varepsilon_\nu = a\,(\alpha) \cdot K_e \cdot B^{\alpha+1} \cdot \nu^{-\alpha} \quad (\text{erg sec}^{-1}\ \text{cm}^{-3}\text{Hz}^{-1}) \tag{5}$$

$a\,(\alpha)$ is a coefficient that depends in a complex way on q. All quantities will be expressed in the CGS system below. In our model, K_e will be determined through DSA theory in the test particle approximation. The most valuable property of this mechanism is the universality of the accelerated particle spectrum, namely, in the test particle approximation it is determined only by the compression ratio across the shock front x_s as $q = \frac{x_s+2}{x_s-1}$, from which the spectral index (4) will also be determined only by x_s:

$$\alpha = \frac{3}{2(x_s - 1)}$$

The compression ratio across the shock is determined by the adiabatic index γ of the local gas and the shock Mach number $M_s = v_s/c_s$:

$$x_s = \frac{\gamma + 1}{\gamma - 1 + 2/M_s^2}$$

In our model, the dependence of the spectrum of radio-emitting electrons on the evolution of the shock wave via the Mach number becomes important. Note that the speed of magnetosonic waves is used as c_s. It is also assumed that at each moment the fraction of accelerated electrons is a fixed fraction of particles from the tail of the Maxwell distribution function behind the shock front.

Integrating over the volume of the source (often over the volume of a sphere), we obtain the luminosity of the SNR

$$L_\nu = \int_V \varepsilon_\nu dV = \int_0^{R_{SNR}} \varepsilon_\nu\,(r) \cdot 4\pi r^2 dr \quad \left(\text{erg sec}^{-1}\text{Hz}^{-1}\right) \tag{6}$$

Using this value, it is possible to calculate the observed characteristics of the radio emission of the SNR, such as the radio flux S_ν and the surface brightness Σ_ν

$$S_\nu = \frac{L_\nu}{4\pi d^2}$$

and

$$\Sigma_\nu = \frac{S_\nu}{\Omega} = \frac{L_\nu}{4\pi^2 R_{SNR}^2}$$

where Ω is the solid angle at which the SNR is observed. It is important to note that the surface brightness does not depend on the distance to the remnant; this parameter is often used when comparing theoretical models with observations. In the 60s of the last century, Shklovsky proposed to use the empirical $\Sigma - D$ relationship to measure distances to SSNs. At that time, the rather scanty statistics of available SNRs showed that developed remnants have a lower surface brightness than young ones; in addition, the young SNR Cas A showed an annual decrease in the radio flux, so the form $\Sigma \propto D^{-\beta}$ was proposed for the $\Sigma - D$ dependence. Many works are devoted to this dependence; on the one hand, it is often used to compare theoretical models of SNR evolution with observations; on the other hand, great hopes were associated with it as a tool for determining distances to supernova remnants. However, many experts are skeptical about $\Sigma - D$ as a tool for determining distances; even the 50% accuracy proposed by the authors of the work [8] can be considered as an overly optimistic estimate.

For young SNRs, it is justified to consider the emissivity as depending only on the radius of the forward shock wave R_s and, when calculating the total luminosity, multiply it by the volume of the layer: $L_\nu = \varepsilon_\nu(R_S) \cdot \triangle V \propto K_e(R_S) \cdot B(R_S)^{\alpha+1} \cdot \triangle V$. Considering $K_e(R_S)$ and $B(R_S)$ to be power-law dependent on the SNR radius, we obtain power-law dependencies $\Sigma \propto D^{-\beta}$ with β values from 3 to 6 and more, sometimes a break is introduced in the $\Sigma - D$ dependence. Unlike young SNRs, for developed supernova remnants it is important to take into account the structure of the remnant, i.e. the total flux of the remnant consists of all the internal layers of the volume that passed the shock wave front at previous moments in time. Figure 2 shows how significant this effect is for developed and old supernova remnants. In this paper, we use the radio emission model proposed by us in paper [1]. This model is based on the assumption that electrons are accelerated from the thermal distribution behind the shock wave front by the DSA mechanism; there is no additional amplification of the interstellar magnetic field; the internal structure is specified in the Cox-Anderson approximation to be able to describe the SNR with a forward shock Mach number of up to two; with the onset of the radiative phase, the generation of new electrons ceases.

Figure 3 shows evolutionary tracks on the $\Sigma - D$ diagram taken from [1] with minor modifications. As can be seen, no power-law dependence of Σ on D is observed while the Mach number of the main shock wave is greater than 10, the dependence of the surface brightness on the diameter is very weak, but with a subsequent sharp drop. Even if all SNRs evolve under the same conditions, this type of evolutionary track does not allow using the $\Sigma - D$ dependence to find the distance by the surface brightness and angular size. In addition to this if we take into account the role of the parameters of both the supernova and the interstellar
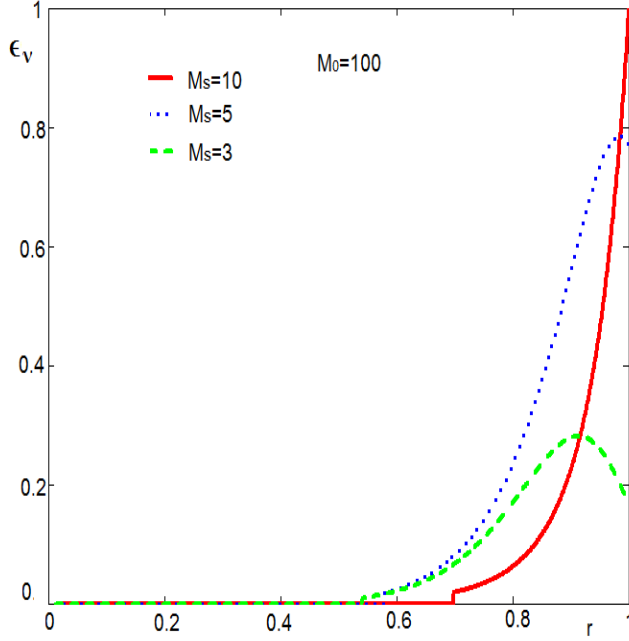
Fig. 2. The evolution of the radial profiles of an undimensional coefficient of emission with M_s.

medium, then the possible spread of these parameters makes it absolutely meaningless to use empirical $\Sigma - D$ dependencies to determine the distances to SNRs. The observational $\Sigma - D$ relations, are mainly due to: 1) presence of SNRs with diameters from wide range of sizes - small diameter bright young SNRs and large size faint old SNRs; 2) D^{-2} effect; 3) selection effects. Unfortunately, it is difficult to check the influence of various selection effects in this problem.

In our model [1], it was assumed that with the onset of the radiative cooling phase, the acceleration of new particles ceases. After this the radio emission of the SNR is provided by electrons accelerated by this moment, the contribution of which, due to adiabatic losses, rapidly decreases without an influx of new particles. In principle, our model with this assumption does not contradict observations, which may mean that the SNR radio emission in the radiative phase is indeed weak. However, it should be noted that the DSA mechanism, as a self-sustaining process, can operate under conditions of the radiative stage of evolution, provided that some not very strict requirements are fulfilled. The first requirement is the presence of a magnetic field and a sufficient degree of ionization in the ISM. The
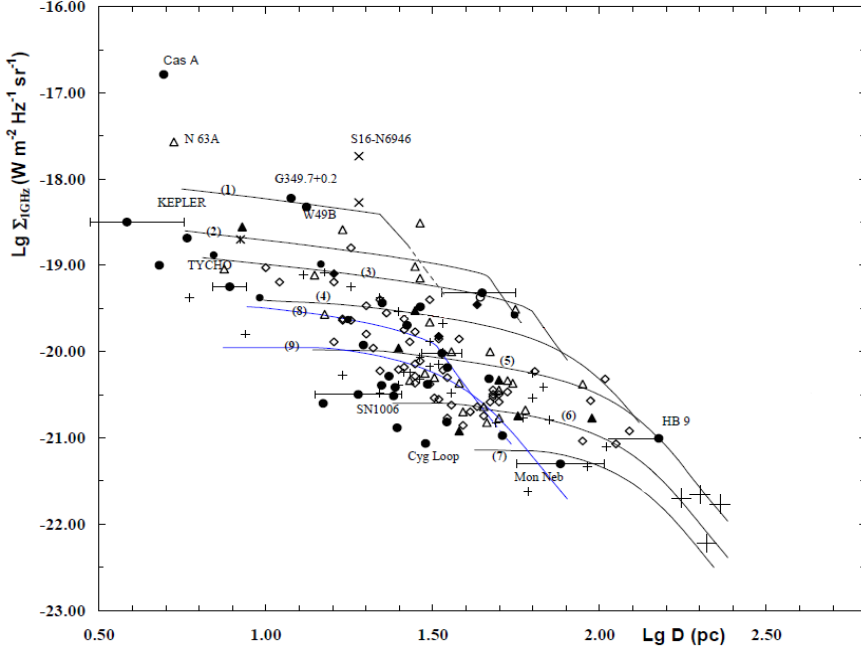
Fig. 3. $\Sigma - D$ tracks from [8] with minor changes.

second requirement is that the characteristic scale of radiative cooling $l_{\rm cool}$ should significantly exceed the characteristic diffusion length $l_{\rm diff}$ of electrons with energies of about GeV: $l_{\rm cool} \gg l_{\rm diff}$. If these conditions are satisfied, then we can apply a simple acceleration model in the test particle approximation. According to [6]

$$l_{\rm cool} \cong 1.0 \cdot 10^{17} \left(\frac{n_0}{1{\rm cm}^{-3}}\right)^{-1} \left(\frac{v_s}{200\ {\rm km} \cdot {\rm s}^{-1}}\right)^{-4} {\rm cm},$$

for shock wave velocities $200\ {\rm km\,s}^{-1} \leq {\rm v_s} \leq 600\ {\rm km\,s}^{-1}$,

$$l_{\rm cool} \cong 10^{19} - 10^{20}\ ({\rm cm}),$$

at $10\ {\rm km\ s}^{-1} < v_s < 200\ {\rm km\ s}^{-1}$

To calculate the diffusion length scale, we will adopt Bohm diffusion ($D_B = vpc/3qB$), and for electrons with energies of 10 GeV we obtain

$$l_{\rm diff} \equiv \frac{D_B}{v_s} \cong 3.3 \cdot 10^{14}\, \eta \left(\frac{B_0}{5\mu G}\right)^{-1} \left(\frac{v_s}{200\ {\rm km} \cdot {\rm s}^{-1}}\right)^{-1} ({\rm cm}),$$

where η is a parameter of the order of unity [10].

As we can see, the condition necessary for the operation of the acceleration mechanism is reliably satisfied for reasonable values of the parameters of the SNR and ISM. At velocities $v_s \geq 200$ km s^{-1} the shock wave itself is able to ionize the plasma around the shell. Thus, the forward shock wave of the SNR at the radiative stage is able to accelerate electrons to energies sufficient to generate synchrotron radio emission.

4. DISCUSSION AND CONCLUSIONS

As can be seen from the distribution of SNRs on the $\Sigma - D$ diagram, there is no dependence of the surface brightness on the diameter, and moreover, it is impossible to explain the observed distribution of supernova remnants by a single power-law dependence of the form $\Sigma = A \cdot D^{-\beta}$. Detailed theoretical models based on complex numerical calculations often predict a power-law form of this dependence (e.g., [2, 7]). This fact does not contradict our statement, since these models are applicable to young SNRs with high shock wave velocities, however, among the observational data on our diagram, the number of young shell-type SNRs is insignificant. Note that a large number of input parameters in such models allows one to obtain the desired or expected result. It should be taken into account that the diffusion acceleration mechanism is a highly nonlinear process, which can have ambiguous results. Therefore, the results of such models should be treated critically and applied to evolved and old SNRs with great caution.

From the analysis of the behavior of evolutionary tracks on the observational $\Sigma - D$ diagram, one can understand the role of various factors in the formation of such a distribution. As we have already stated, this diagram is practically unsuitable for determining distances to remnants. The main observational properties of observed SNRs in the radio range can be easily explained within the framework of the DSA mechanism. In this case, the evolutionary tracks have a universal character if the Mach number is taken as the value describing the evolution of SNRs. Then, regardless of whether the radiative phase begins or the evolution occurs adiabatically until the end of life, the DSA mechanism operates on the main shock wave, accordingly, the radio life is determined by the Mach number. Of course, old SNRs cannot be considered important accelerators of high-energy cosmic rays, but the process of particle acceleration in them continues. This issue was studied in detail in the work [11]. The best proof of the correctness of our idea that at the radiative stage the process of radio emission continues due to the work of DSA on the outer shock wave would be the detection of radio emission from the very edge of the SNR with $\alpha \geq 0.6$. However, such observational detection will be associated with great difficulties due to the weakness of the emission from the

thin region, in the presence of inhomogeneities and irregularities characteristic of old objects.

REFERENCES

1. Asvarov A.I., 2006, A&A, **459**, 51

2. Berezhko E.G., & Völk H.J., 2004, A&A, **427**, 525

3. Bertschinger E., 1986, ApJ, **304**, 154

4. Cox D.P., & Anderson P.R., 1982, ApJ, **253**, 268

5. Green D.A., 2024, arXiv preprint , arXiv:2411.03367

6. McKee C.F., & Hollenbach, D.J., 1980, ARA&A, **18**, 219

7. Pavlović M.Z., Urošević D., Arbutina B., 2018, et al., ApJ, **852**, 84

8. Ranasinghe S., Leahy D., 2023, ApJS, **265**, 53

9. Sedov L. I., 1977, Similarity methods and dimensional analysis in mechanics, in Russian, Moscow: Nauka

10. Vink J., 2020, Physics and Evolution of Supernova Remnants, 519

11. Zirakashvili V.N., & Ptuskin, V.S., 2022, MNRAS, **510**, 2790

)

IMPACT OF THE COSMOLOGICAL CONSTANT ON THE EVENT HORIZON

B. A. Rajabov [a*]

[a] *Shamakhy Astrophysical Observatory named after N.Tusi of Ministry of Science and Education of the Republic of Azerbaijan, Shamakhy, Azerbaijan*

Schwarzschild's solution for Einstein's equations in the case of a non-zero cosmological constant is considered. Observations show that the cosmological constant is different from zero. Therefore, the study of such solutions is necessary. It is shown that the dependence of the event horizon on the cosmological constant is discontinuous. The event horizon exists for zero and negative values of the cosmological constant of the central spherically symmetric body.
Keywords: cosmological constant – event horizon – Schwarzschild solution – Einstein's equations.
AMS Subject Classification: 20-20C, 33-33C, 83-83F, 81-81E

1. INTRODUCTION

According to Einstein's concept, space-time geometry is determined not a priori, but by the motion and distribution of matter, and gravitational phenomena were identified with the non-Euclidean geometric structure of space-time. Einstein showed that the local principle of equivalence of gravitational and inert mass in combination with the principle of relativistic invariance with the necessity of leads to field theory and Riemann's geometry), and the metric tensor components play the role of gravitational potential, [1, 8, 9]:

$$R_{ik} - \frac{1}{2} g_{ik} R = \varkappa T_{ik}. \tag{1}$$

---

[*] E-mail: balaali.rajabov@mail.ru

)More precisely, pseudo-Riemannian geometry, since the g_{ik}−metric of space-time has the signature $(+1, -1, -1. -1)$. Only geometries with a positive-definite quadratic form are called Riemann manifolds.

The constant $\varkappa$ is related to the gravitational constant k as the following relationship:

$$\varkappa c^2 = 8\pi k/c^2 = 1,87 \cdot 10^{-26} \text{m/kg},$$

where $c-$ is the speed of light in a vacuum.

After the creation of the foundations of the general theory of relativity, A. Einstein proceeded to solve cosmological problems. In connection with cosmological problems, he proposed gravitational equations with the cosmological "$\Lambda-$term", [1,4,9]:

$$R_{ik} - \frac{1}{2} \, g_{ik}R + \Lambda g_{ik} = \varkappa T_{ik}. \tag{2}$$

Observations show that the cosmological constant Λ is different from zero. Therefore, the study of such solutions is necessary.

2. SCHWARZSCHILD'S SOLUTION AND THE GRAVITATIONAL RADIUS

The first exact solution was found by Schwarzschild in 1916. The linear element according to the Schwarzschild solution has the form, [3]:

$$ds^2 = \left(1 - \frac{2M}{r}\right) dt^2 - \frac{dr^2}{1 - 2M/r} - r^2 \left(d\theta^2 + \sin^2\theta d\varphi^2\right). \tag{3}$$

As can be seen, this solution represents a static and spherically symmetric field.

A similar solution for a static and spherically symmetric field can be written in the case of the Einstein equation eq.(2) with a cosmological term, [3]:

$$ds^2 = \left(1 - \frac{2M}{r} - \frac{\Lambda}{3}r^2\right) dt^2 - \frac{dr^2}{1 - 2M/r - \Lambda r^2/3} - r^2 \left(d\theta^2 + \sin^2\theta d\varphi^2\right). \tag{4}$$

These solutions are called the outer Schwarzschild solutions.

The Schwarzschild solution with $\Lambda = 0$, eq.(3) has a singularity at radius and valid only outside this radius:

$$r_g = 2M. \tag{5}$$

Since the parameter r_g has the dimension of mass, both solutions are interpreted as a field surrounding the gravitating body, and r_g is called its gravitational or Schwarzschild radius.

As long as the real radius of the body is greater than its gravitational radius, there are no obstacles to applying the Schwarzschild solution$^{)}$. But at present,

---

$^{)}$For the Sun, the Schwarzschild radius $r_{0\odot} = 2.95 \; km$, i.e. is deep within it. For the Earth, the gravitational radius $r_{g\oplus} = 8.87 \; mm$. And for the proton, the Schwarzschild radius

cosmological objects are known to be entirely within their Schwarzschild radius. They are called *Black holes*. It is known for certain that at the centers of galaxies and quasars, as a rule, there are black holes, even binary systems of black holes.

The Schwarzschild radius is not a singularity and is called the *event horizon* or the *surface of a black hole* and is also called the *static limit*. The fate of the collapsing matter after it crosses the surface of the black hole is unknown. No radiation or matter can escape a black hole.

The Schwarzschild solution corresponds to a non-rotating non-charged black hole.

Similarly, the equation for the gravitational radius at a non-zero cosmological constant is determined by the singularity of the solution from (4):

$$1 - \frac{2M}{r} - \frac{\Lambda}{3}r^2 = 0. \tag{6}$$

This equation is reduced to an equation of the third degree:

$$\Lambda r^3 - 3r + 6M = 0$$

and is solved by the Cardano method, [2], (see Appendix).

For $\Lambda \neq 0$ it has two complex and one real solution. We are, of course, interested in a real solution that has a physical meaning. By this solution, the dependence of the gravitational radius on the cosmological constant is given by a discontinuous function of the following form:

$$r_g = \begin{cases} 2M, & \text{if} \quad \Lambda = 0, \ M \neq 0, \\ \kappa/\Lambda + 1/\kappa, & \text{if} \quad \Lambda \neq 0, \end{cases} \tag{7}$$

where

$$\kappa = \left(-3M\Lambda^2 + \Lambda\sqrt{9M^2\Lambda^2 - \Lambda}\right)^{1/3}.$$

By direct substitution, one can verify that (7) is a solution to (6).

The condition of positivity of the gravitational radius r_g is possible in two cases:

1. if $\Lambda < 0$ then $M > 0$;

2. if $\Lambda > 0$ then $9M^2\Lambda > 1$ and $M < -M_g < 0$, where

$$M_g \equiv \frac{1}{3\sqrt{\Lambda}}. \tag{8}$$

We remind you that M is the constant of integration of the Einstein equations.

is 10^{-59} *cm*, which is 37 orders of magnitude smaller than its characteristic radius of 10^{-13} *cm*, [9].

3. CONCLUSIONS

Further analysis of the obtained dependence of the gravitational radius on the cosmological constant leads to interesting conclusions. Obvious physical considerations require that the gravitational radius be a positive value: $r_g > 0$.

The parameter M takes positive values for the Schwarzschild interval without the cosmological term (3) and is interpreted as the mass of the gravitating body.

For a Schwarzschild interval with a cosmological term (4), negative values of M lead to a different interpretation. As shown in [5–7], negative mass or energy, which is the same, can be interpreted as *Dark energy*, which is a *Cosmological quantum effect*. Therefore, this solution cannot be excluded when considering quantum effects in cosmology.

APPENDIX

In the appendix, we present a direct application of the Cardano method to eq.(6).

In case $\Lambda \neq 0$, eq.(6) can be reduced to the form:

$$r^3 - \frac{3}{\Lambda}r + \frac{6M}{\Lambda} = 0. \tag{9}$$

To further simplify this equation, we introduce a couple of new variables (u, v) using the substitution $r = u + v$:

$$u^3 + v^3 + \left(3uv - \frac{3}{\Lambda}\right)(u + v) + \frac{6M}{\Lambda} = 0$$

An additional condition can be imposed on variables (u, v):

$$3uv - \frac{3}{\Lambda} = 0.$$

Then for the unknowns (u, v) we obtain the following equations:

$$u^3 + v^3 = -\frac{6M}{\Lambda}; \qquad u^3 v^3 = \frac{1}{\Lambda^3}. \tag{10}$$

According to the theorem of Viet, variables (u^3, v^3) are solutions of the following square equation:

$$x^2 + \frac{6M}{\Lambda}x + \frac{1}{\Lambda^3} = 0. \tag{11}$$

The solutions of the quadratic equation (11) are well known:

$$u^3 = -\frac{3M}{\Lambda} + \sqrt{\left(\frac{3M}{\Lambda}\right)^2 - \frac{1}{\Lambda^3}},$$

$$v^3 = -\frac{3M}{\Lambda} - \sqrt{\left(\frac{3M}{\Lambda}\right)^2 - \frac{1}{\Lambda^3}}. \tag{12}$$

From the last levels one can obtain an explicit expression for the gravitational radius $r = u+v$. When taking cube roots, it is necessary to ensure that conditions (10) are met. We omit the details of the calculations.

REFERENCES

1. Einstein A., 1965, Collected Works, Nauka, Moscow

2. Granino K.A. & Theresa K.M., 1961, Mathematical Handbook for Scientists and Engineers, McDraw-Hill Book Company, Inc.

3. Kramer D., Stephani H., Maccallum M. & Herlt E., 1980, Exact solutions of the Einstein's field equations (Schmutzer E., ed.), Deutscher Verlag der Wissenschaften, Berlin

4. Moeller C., 1972, The theory of relativity, Clarendon Press, Oxford

5. Rajabov B.A., 2018, A&AC, **3**, 74

6. Rajabov B.A., 2020, J. Sci. & Tech., ICONAT 2020 Special Issue, **21**, 128

7. Rajabov B.A., 2022, AzAJ, **17**, 62

8. Tolman R.C., 1969, Relativity, Thermodynamics and Cosmology, Clarendon Press, Oxford

9. Weinberg S., 1972, Gravitation and Cosmology, John Wiley and Sons, Inc., New York–London–Sydney–Toronto

)

PHOTOMETRIC OBSERVATIONS OF HIGH MASS X-RAY BINARY HD 226868

J. N. Rustamov [a*], *A. R. Iskandarova* [a], *E. A. Gurbanov* [a],

U. J. Poladova [a]

[a] *Shamakhy Astrophysical Observatory named after N.Tusi of Ministry of Science and Education of the Republic of Azerbaijan, Shamakhy, Azerbaijan*

The results of photometric observations of the high mass X-ray binary HD 226868 = Cyg X-1 have been presented. The observations of this star were performed at 60-cm telescope of ShAO named after N.Tusi by using CCD photometer. This star is a binary system consisting of a black hole and a massive giant component star. Black hole and optical giant component masses are $M = 20 \pm 5 M_\odot$ and $M_{opt} = 40 \pm 5 M_\odot$, respectively. The blue supergiant orbiting the black hole is HDE 226868 and its spectral type is O9.7 Iab. Our aim was investigating variability of this star in the V filter of the BVRI photometric system. Together with our photometric observations we used also AAVSO photometric database for the star HD 226868. Short-term and long-term photometric variability of this star has been revealed. The low luminosity state of star HD 226868 was discovered by analyzing the AAVSO photometric database, where V magnitude changes in the interval between $\sim 9^m.1$ and $9^m.2$. The lower luminosity state was observed on November 16, 2021, from $19^h 55^m 12^s$ to $20^h 11^m 02^s$. This state may be related to the supergiant wind instability as well as changes in the supergiant's mass transfer rate.

Keywords: high-mass X-ray binary – binary star systems – photometric variability – HD 226868

1. INTRODUCTION

The star HD 226868 = Cyg X-1 is a High-Mass X-ray Binary (HMXB), which was the first identified bright X-ray source [5, 19, 29]. HMXBs were among the

very first bright X-ray sources detected in the 1970s. The identification of the single-lined supergiant star HD 226868 with the X-ray source Cyg X-1 was reason to believe that this star is a binary system where the secondary component is a neutron star or a black hole. Cyg X-1 was the first close binary system in which the presence of a black hole was revealed [5, 29] and it was the only object of that type for about a decade. Its studies are important for the understanding of the evolutionary properties of massive stars, the formation of black holes and neutron stars in these systems, processes of accretion onto black holes in close binary systems and also for the testing massive stars evolution models. Another high importance investigation of these objects is connected with the fact that, the HMXBs are potential progenitors of gravitational wave sources. Studying the Galactic HMXB population can provide valuable insights into their formation and evolution.

HMXBs are binary systems consisting of a compact object, either a black hole or a neutron star, and a high-mass optical component (supergiant) with a mass greater than $8M_\odot$ [7]. These systems emit X-rays due to the accretion of material from the optic companion star, which heats up as it falls onto the compact object. The material transfer can occur via stellar winds or Roche-lobe overflow, producing X-ray luminosities ranging from 10^{35} to 10^{38}erg/s [7].

The star HD 226868 consists of supergiant optic component with the spectral type O9.7 Iab. [28] and a black hole. Although many different models were proposed for this star to avoid the presence of a black hole, at present, there are no doubts about the presence of a black hole in this system. The orbital period of this binary system is $\sim 5.6^d$ [5,29]. The spectral type of this star was determined for the first time in [28] as O9.7 Iab and confirmed by the authors of [10,13,20]. In [13] by using the atmosphere models obtained the value 32000 K for the effective temperature of HD 226868.

Although more than three decades discovering of the star Cyg X-1, the masses of the components in this binary system are still a subject of controversy, there is still substantial uncertainty concerning the masses of both components. The most recent and precise value of mass function of optical component is $f(M_x) = 0.251 \pm 0.007 M_\odot$ [12]. Although the mass function of the optical star is relatively small, it is tens of times larger than the mass function values for the corresponding binary systems with X-ray pulsars [7].

Because of the uncertainty of the orbital inclination, the mass of the secondary component was unknown. However, the minimum mass estimates in [12,13] make it reasonable to suggest that the secondary component is a black hole. The masses of the components have been determined as $17.8M_\odot$ for the supergiant and $10.1M_\odot$ for the black hole [13].

By analyzing the emission lines of the stellar wind, the rotational broadening of the absorption lines of the optical component and the photometric V-band light curve, authors of [10, 11] conclude that the optical component is close to filling its Roche lobe, the fill-out factor is close to 1 and according to [31] the best value for the fill-out factor is in the range 0.95-1 [31].

From the analysis of rotational broadening of the absorption lines of the optical component and the ellipsoidal light variations of V-band light curve the authors of [10, 11] received the value of $33^0 \pm 5^0$ for the inclination of the orbit.

If the distance to the HD 226868 is in the range of $1.95 - 2.35$ kpc and the effective temperature is in the range $30000 - 31000$ K , then the mass of optical component has to be in the range of $40 \pm 5 M_\odot$ [31]. By analyzing the profiles of the emission lines, rotational broadening of the absorption lines and the ellipsoidal light variations, obtained the value of $20 \pm 5 M_\odot$ for the mass of the black hole component [31].

The light variations with the small amplitude ($\Delta V \sim 0^m.04$) with a ~ 5.6-day orbital period were revealed in [17, 18, 26]. The light curve of star HD 226868 can be explained by tidal deformation of the supergiant component by the gravitational field of black hole, which is surrounded by an accretion disk [18].

The different longer periods (294 days, 150 days, and 4.5 years) were revealed for the Cyg X-1, which is thought to originate from an oblique accretion disk precession due to gravitational torques from the supergiant component [15, 21, 29]. However, the ~ 5.6 day orbital period is the only one that is confirmed in all wavebands by most authors. It has been suggested that the 294 day period is aliasing of the true 150 day period [21].

Authors of [13] during the high (soft) state of the X-ray source of Cyg X-1 in April-May 1975, revealed the oscillations in the light curve with a period of 61.9 minutes. $39^d.2, 78^d.4, 149^d.4$ and $53^d.3$ periodicities were also detected in [15, 27].

Light periodicity analysis of HD 226868 is complicated because the optical light variations are small and irregular variability is superimposed on the light curve. The photometric behavior of star HD 226868 is quite complex. The light curve is similar to the light curve of distorted binaries, with the considerable additional intrinsic variability. The large scatter in light variations explains with the intrinsic variability of supergiant component. But may be takes place also variable obscuration by irregular gas streams. The intrinsic variability of supergiant component is recognized as a characteristic of this star by all observers and some of the unusual photometric features may be connected with this. In [13] another peculiarity of the light curve was revealed: an extremely rapid rise in brightness on the ascending side of both light minima.

High X-ray luminosity ($2 - 5.5 \cdot 10^{37}$ erg/s) and significant emission of gamma rays are the observational facts that favor for the presence of an accretion disk harboring Cyg X-1 [2, 4, 25]. The X-ray spectrum of Cyg X-1 is consists of blackbody and power law components. The blackbody component comes from the accreting disc and power law component generates by Compton scattering of disc emission by either a hot corona of electrons or at the base of a jet [3, 6, 23]. The existence of highly collimated jet observed in [24] and confirmed in [8].

The X-ray luminosity of Cyg X-1 observed in two spectral states: low (hard) and high (soft). The star Cygnus X-1 about 90% of the time is in low (hard) state [9]. To the low (hard) state corresponds relatively low accretion rate from the supergiant component and because relatively low X-ray luminosity. The low accretion rate in the low (hard) state allows the optically thick, but geometrically thin disk to be evaporated more efficiently. An optically thin, hot corona of electrons flows from the disk inner radius to the event horizon of black hole component. This corona generates the power law low (hard) spectrum [9]. Occasionally, the mass accretion rate from the supergiant component slightly increases, by only $\sim 15\%$ [17], which causes an increase in X-ray luminosity of about 10% to 20% [6]. Evaporation of the disk proceeds less efficiently in the high/soft state, and the disk inner radius advances to the last stable orbit of the black hole. This causes the disk blackbody emission to dominate over the power law radiation from the corona [6].

It should be note that the complexity in the Cygnus X-1 system is very high, even during the low (hard) state and during the high (soft) state, additional events are introduced.

2. OBSERVATIONAL DATA, THEIR REDUCTION AND RESULTS

Photometric observations of the HMXB star HD 226868 were carried out during 2020-2022 years, at the 60-cm Zeiss telescope of the Shamakhy Astrophysical Observatory (ShAO) named after N. Tusi, equipped with a CCD photometer, in the V filter of the BVRI photometric system [1]. The MaxIM DL program was used to process the obtained CCD images. The standard star HD 226867(V = 10^{m}.7) and two control stars, HD 226938 (V = 10^{m}.14) and HD 226919 (V = 9^{m}.56), were used. The root mean square error of photometric observations determined by using the control star is 0.007 . Table 1 presents information concerning our photometric CCD observations of HD 226868. In this table were shown: the date of observations, number of received CCD images obtained during one night (N), exposure time in seconds. Obtained also flat field, dark and bias images for the processing CCD images of star HD 226868.

Table 1. The photometric CCD observations of HD 226868 at 60-cm telescope of ShAO.

| 2020	N	Exp (sec.)	2021	N	exp	2022	N	Exp (sec.)
06 23/24	300	8	05 12/13	50	10	07 08/09	150	7
0624/25	180	6	05 15/16	300	10	07 17/18	100	10
07 17/18	250	12	06 01/02	100	10	07 18/19	150	10
07 24/25	188	10	06 17/18	150	15	07 19/20	100	10
07 26/27	258	10	06 18/19	150	8			
07 27/28	200	10	06 19/20	150	13			
			07 04/05	150	10			
			07 18/19	150	10			
			09 02/03	50	20			
			09 13/14	157	10			
			09 16/17	120	8			
			11 09/10	200	8			
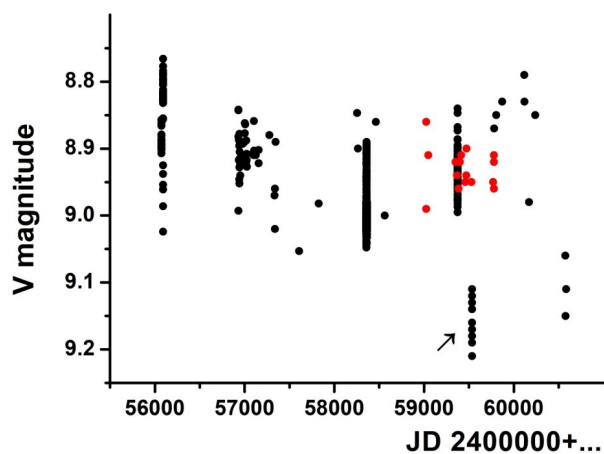
Fig. 1. V magnitude variations of star HD 226868 from May 26, 2012 to September 30, 2024. The red and black dots represent our and AAVSO dates, respectively..

The American Association of the Variable Stars Observations (AAVSO) [32] high accuracy photometric database of HD 226868 was used to reveal short-term and long-term photometric variations (Fig. 1-Fig. 3).

Fig. 1 shows V magnitude variations of HD 226868 during 2012-2024. The red and black dots represent our and AAVSO dates, respectively. The arrow in Fig. 1 indicates the lower luminosity state of star HD 226868, where V magnitude changes in the interval between $\sim 9^m.1$ and $9^m.2$. Lower luminosity state was on
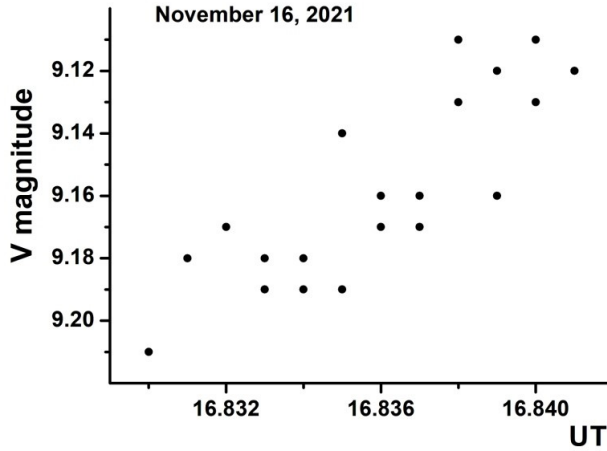
Fig. 2. V magnitude variation of star HD 226868 plotted by using AAVSO observations Database,on November 16, 2021.
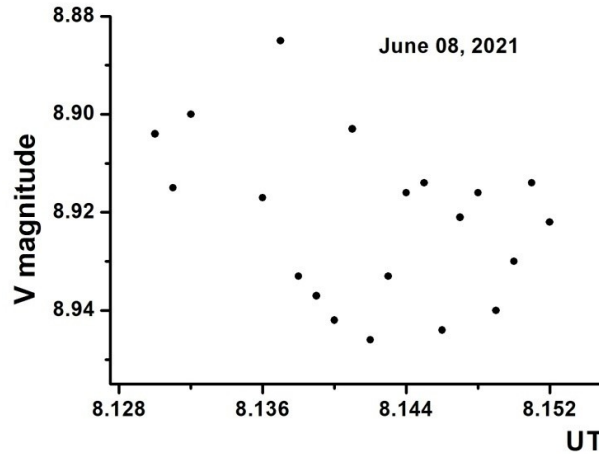
Fig. 3. V magnitude variation of star HD 226868 plotted by using AAVSO observations Database, on June 08, 2021.

November 16, 2021, from $19^h55^m12^s$ to $20^h11^m02^s$. ($\sigma = 0.012$). As seen in Fig. 1 the star HD 226868 was only once in this state during 2012-2024. Revealing the low luminosity state on November 16, 2021, is real because of the existence of high-precision ($\sigma = 0.012$) eight measurements. The low luminosity state may be connected with the long-term photometric variability or with the wind instability of the supergiant component.

Fig. 2 shows the V magnitude variation of star HD 226868 plotted by using AAVSO observations database ($\sigma = 0.012$) on November 16, 2021.

Fig. 3 shows the V magnitude variation of star HD 226868 plotted by using AAVSO observations database ($\sigma = 0.003$) of star HD 226868 on June 8, 2021, for 34 minutes, from $03^h04^m30^s$ to $03^h38^m46^s$ UT.

As seen from Fig. 2 and Fig. 3, the rapid photometric variations of star HD 226868 were observed. Revealed the low luminosity state of this star (arrow in Fig. 1) may be related to the supergiant wind instability as well as changes in the supergiant's mass transfer rate.

3. CONCLUSIONS

The main result of this research is revealing the low luminosity state of star HD 226868, where V magnitude changes in the interval between $\sim 9^m.1$ and $9^m.2 (\sigma = 0.012)$. The lower luminosity state was observed on November 16, 2021, from $19^h55^m12^s$ to $20^h11^m02^s$. In future research, it is reasonable to clarify the relation of this state to the low (hard) and high (soft) stages of X-ray luminosity of HD 226868. This observational fact is important in constructing the physical model of star HD 226868. Low luminosity state may be related to the supergiant wind instability as well as changes in the supergiant's mass transfer rate.

4. ACKNOWLEDGMENTS

REFERENCES

1. Abdullaev B.I., Gulmaliev N.I., Mejidova S.O., et al., 2009, AzAJ, **4**, 41

2. Albert J., Aliu E., Anderhub H., et al., 2007, ApJ, **665**, L5

3. Balucinska-Church M., Belloni T., Church M.J., et al., 1995, A&A, **302**, L5

4. Balucinska-Church M., Church M.J., Charles P.A., et al., 2000, MNRAS, **311**, 861

5. Bolton C.T., 1972, Nature, **235**, 271

6. Brocksopp C., Fender R.P., Larionov V., et al., 1999, MNRAS, **309**, 1063

7. Cherepashchuk A.M., 2013, Close Binary Stars, V1, Moscow Fizmatlit

8. Fender R.P., Stirling A.M., Spencer R.E., et al., 2006, MNRAS, **369**, 603

9. Gallo E., Fender R., Kaiser C., et al., 2005, Nature, **436**, 819

10. Gies D.R., Bolton C.T., 1986a, ApJ, **304**, 371

11. Gies D.R., Bolton C.T., 1986b, AJ, **304**, 389

12. Gies D.R., Bolton C.T., Thomson J.R., et al., 2003, ApJ, **583**, 424

13. Herrero A., Kudritzki R.P., Gabler R., et al., 1995, A&A., **297**, 556

14. Kemp J.C., Herman L.C., Barbour M.S., 1978, AJ, **83**, 962

15. Kemp J.C., Herman L.C., Rudy R.J., et al., 1977, Nature, **270**, 227

16. Kemp J.C., Karitskaya E.A., Kumsiashvili M.I., et al., 1987, Soviet AZh, **31**, 170

17. Lester D.F., Nolt I.G., Radostitz J.V., 1973, Nature Phys. and Sci., **214**, 125

18. Lyuty V.M., Sunyaev R.A., Cherepashchuk A.M., 1973, Soviet AZh, **17**, 1

19. Lyuty V.M., Sunyaev R.A., Cherepashchuk A.M., 1973, AZh, **50**, 3

20. Ninkov Z., Walker G.A. H., Yang S., 1987, ApJ, **321**, 425

21. Ozdemir S., Demircan O., 2001, Astron. and Space Sci., **278**, 319

22. Pooley G.G., Fender R.P., Brocksopp C., 1999, MNRAS, **302**, L1

23. Shapiro S.L., Lightman A.P., Eardley D.M., 1976, AJ, **204**, 187

24. Stirling A.M., Spencer R.E., de la Force C.J., et al., 2001, MNRAS, **327**, 1273

25. Syunyaev R.A., Trümper J., 1979, Nature, **279**, 506

26. Walker E.N., 1972, MNRAS, **160**, 9P

27. Walker E.N., Quintanilla A.R., 1978, MNRAS, **182**, 315

28. Walborn N.R., 1973, ApJ, **179**, L123

29. Webster B.L., Murdin P., 1972, Nature, **235**, 37

30. Wilson R.E., Fox R.K., 1981, AJ, **86**, 1259

31. Ziolkowski J., 2005, MNRAS, **358**, 851–859

32. https://www.aavso.org/

)

DYNAMICAL EVOLUTION AND STATISTICS OF DAMOCLOIDS. 2.

A. S. Guliyev [a*], *R. A. Guliyev* [b], *V. V. Kleshchonok* [b],

N. S. Kovalenko [c]

[a] *Shamakhy Astrophysical Observatory named after N.Tusi of Ministry of Science and Education of the Republic of Azerbaijan, Shamakhy, Azerbaijan*

[b] *Astronomical Observatoria of Kyiv Shevchenko National University, Kyiv, Ukraine*

[c] *Ukraine Ministry of Education and Science of Ukraine Ukrainian State Center for International Education, Dragomanov Ukrainian State University, Ukraine*

This paper presents a comparative analysis of two small-body populations: Damocloids and long-period comets, covering 171 and 1495 objects, respectively. It is established that, on average, Damocloids have larger perihelion distances. The inclination distributions are quite similar for both systems, with retrograde motion predominating. A striking difference is found in the comparison of perihelion concentration planes. Unlike long-period comets, the perihelia of Damocloids tend to concentrate more toward the ecliptic. In the distribution of MOID values of Damocloids and long-period comets relative to the orbits of the giant planets, excesses are observed in both groups, being more pronounced among Damocloids.

Keywords: damocloids – long-periodic comets – giant planets – statistics

1. INTRODUCTION

The present article is a logical continuation of the work [8], which analyzed the structure and evolutionary characteristics of the Damocloid population. These are minor bodies following comet-like orbits but lacking visible coma. The Tisserand parameter values relative to Jupiter, do not exceed two. The cited study examined the orbital evolution of 144 such objects. The results obtained in that work

* E-mail: quliyevayyub@gmail.com

provide a basis for expanding the scope of the analysis of the Damocloid system and exploring new patterns within this population of small bodies.

2. OBJECTIVE OF THE STUDY AND DATA USED

Since most Damocloids originate from outer regions of the Solar System, it is natural to hypothesize their similarity to long-period comets. In other words, Damocloids may represent comets that have lost their volatile components and evolved into asteroid-like bodies. Their relatively large sizes might be explained by selection effects. If this scenario holds true, there should be significant similarities between Damocloids and LPCs in terms of their orbital characteristics (e.g., orientation of apsidal lines, perihelion concentration near particular points or planes on the celestial sphere-great circles on the celestial sphere aphelion and nodal distances, etc.). This question was partially addressed in a previous study, but that analysis was not exhaustive. Thus, this subject requires further investigation, which constitutes one of the objectives of the present paper.

Furthermore, the number of identified Damocloids has significantly increased in recent years, expanding the possibilities for deeper analysis. As of early 2025, the number of such bodies has reached 316, which is 2.2 times higher than during the period covered in study [8]. In this study, the authors aim to compare two minor-body populations: Damocloids and LPCs. A constraint on aphelion distances $Q>30AU$ has been set for both small-body populations. It is reasonable to assume that objects with lower Q values are more strongly influenced by the gravitational perturbations of giant planets. The number of Damocloids meeting this criterion is 171. The compiled list begins 5335 Damocles (1991 DA) and ends with (2024 XN25). Additionally, a small number of rare objects with perihelion distances $q>10$ AU were excluded from further consideration to ensure the robustness of the analysis.

Regarding LPCs, three additional restrictions were applied:

1. Comets with perihelion distances $q<0.01AU$ were excluded from the list.

2. If multiple LPCs have nearly identical orbits (twin comets) only one is included in the dataset. For example, comets C/1988 F1 and C/1988 J1 share almost identical orbits and are likely fragments of a common parent nucleus. In a comparative analysis, it is more reasonable to consider them as single entity. This effect is even more pronounced among short-perihelion comets, which are therefore entirely excluded from the statistical sample.

3. As with Damocloids, comets with $q>10AU$ were also excluded from consideration. As previously noted, their numbers are extremely small, yet they could distort the statistical similarities or differences being investigated.

A review of the comet catalog [9] and MPEC data up to early 2025 resulted in a dataset of 1495 objects for comparative analysis. This list begins with comet C/-43 K1 and ends with C/2024 Y1.

3. FEATURES OF THE DISTRIBUTION OF APHELION DISTANCES OF DAMOCLOIDS

It is well known that the distribution of aphelion distances (Q) for long-period comets (LPC) in the trans-Neptunian region exhibits certain clustering and "gaps". This phenomenon has been recognized for a long time (see, for example, [4,5]) and has even been utilized in attempts to predict undiscovered planetary bodies in the Solar System. These clusters are particularly prominent in the ranges of 30–38 AU, 49–57 AU, 73–89 AU, 99–117 AU, and 160–180 AU. In this respect, the data for Damocloids independently or simultaneously raise interest. The authors analyzed the values of Q for 171 Damocloids and noted that only the clustering within the range of 101–120 AU, (18 objects), warrants further investigation, as the adjacent intervals contain

only 10 and 5 objects, respectively. No similar clustering or gaps are observed across the rest of the distance scale. Analysis and calculations showed that the aphelia of 8 out of the identified 17 Damocloids are concentrated within $\pm 10°$ of the plane defined by parameters:

$$\mathrm{I_p} = 11^0.40 \cdot \Omega_p = 331^0.49 \tag{1}$$

Some data regarding these 8 Damocloids are provided in the left part of Table 1. The concentration of perihelia near this plane is statistically significant and unlikely to be accidental. A parallel analysis of long-period comets with Q ranging from 100 to 120 AU revealed a rather intriguing pattern. It turned out that the perihelia of 8 out of 27 such comets, observed up to early 2025 , are located within $\pm 10°$ of the plane with the following parameters:

$$\mathrm{I_p} = 10^0 \cdot \Omega_\mathrm{p} = 358^0 \tag{2}$$

A list of these comets along with some of their data is presented in the right part of Table . Although this concentration is less pronounced than the previous one, the proximity of the parameters of the computed planes remains noteworthy.

The observed similarity between these two classes of minor bodies corresponding to the same Q range should be further investigated as new objects are discovered. It is possible that this similarity contains valuable information for theoretical searches of undiscovered planetary bodies.

Table 1. Parameters of 8 Damocloids and 8 LPCs relative to two planes

Some Damocloids parameters relatively to the plane (1)				Some comet parameters relatively to the plane (2)			
Damocloid	q	e	B'	Long-period comets	q	e	B'
(2000 AB229)	2.273	0.956	2.11	C/2005 O1	3.591	0.93	-9.95
(A/2020 B1)	1.748	0.967	-1.49	C/1995 Q2	1.889	0.967	-6.44
(2024 LY9)	9.679	0.839	-4.9	C/1964 N1	0.822	0.985	-4.21
(2024 RQ11)	2.675	0.954	-4.49	C/2013 PE67	1.847	0.967	-3.77
(A/2019 Q2)	1.258	0.979	-4.6	C/2020 Q1	1.315	0.978	-1.35
(2020 KX11)	3.244	0.947	2.1	153P/1661 C1	0.513	0.99	7.64
(2016 AT281)	2.688	0.956	-9.57	C/2007 D2	1.245	0.977	9.33
(2012 HD2)	2.534	0.959	-5.85	C/1941 B1	0.942	0.981	9.45

4. FEATURES OF THE DISTRIBUTION OF ORBITAL APSIDAL LINES

The peculiarities of the distribution of perihelion longitudes (and consequently, aphelion longitudes) have long formed the basis for various hypotheses in cometary cosmogony [4]. In this section, we primarily aim to determine the extent to which Damocloids resemble long-period comets (LPCs) in this regard. As is well known, the perihelion longitude of a comet or Damocloid is calculated using the formula:

$$L = \Omega + \operatorname{atan}(\tan\omega\cos i)$$

where Ω, ω, and i are the angular orbital elements. However, in some studies, particularly in meteor astronomy, authors often use a simpler formula:

$$\pi = \Omega + \omega \qquad (3)$$

Since we are only comparing two small-body systems, we will adopt the aforementioned formula (3). By dividing the range of possible values into 12 intervals, we counted the numbers of comets and Damocloids in each. After applying the appropriate normalization, we employed the Kolmogorov-Smirnov test to compare the perihelion distributions. [2, 10]. It turned out that the test statistic is 0.55, and its significance is well below than the required 95% confidence level. This indicates that perihelion distributions of Damocloids and LPCs do not differ greatly. It is known that the perihelia of LPCs are concentrated around two planes (great circles on the celestial sphere), which have a mutual inclination of about 80° [6]. These planes are inclined relative to the ecliptic by 40.2° and 86.2°, respectively,

with the concentration near the-latter being more pronounced. This observation has provided the basis of for the hypothesis of a large trans-Neptunian planet. Calculations conducted using the methodology described in [6] demonstrate that the perihelia or aphelia of Damocloids concentrate near a plane with the following parameters:

$$I_p = 5^0.32; \Omega_p = 342^0.36 \qquad (4)$$

For instance, the orbits of 30 Damocloids have latitudes ranging from $-5°$ to $+5°$ relatively (4). This represents an initial marked difference from the long-period comets. There is one more characteristic of LPCs that can be tested in the Damocloid system. Such comets exhibit an excess of aphelia in the range of 250 to 400 AU [6]. Analysis of individual Q values for Damocloids demonstrates no distinct excess within this interval, although 9 values are concentrated between 280-360 AU. The optimal plane of perihelia for these selected 9 objects has the following parameters:

$$I_p = 85^0.53 \cdot \Omega_m = 78^0.14 \qquad (5)$$

A rather weak similarity with long-period comets is observed here, as the two planes (the plane calculated in [6] and (5))have a mutual inclination of approximately 28°. However, the deviations of perihelia of these nine comets from plane (5) span a considerable range. With only three comets exhibiting deviations within ±10°. Therefore, it must be concluded that Damocloids significantly deviate from long-period comets in terms of perihelion distribution. Their perihelia tend to be more concentrated toward the ecliptic.

5. COMPARISON OF TWO SYSTEMS BY PERIHELION DISTANCES

Calculations show that the Damocloids from the compiled list have the following q_{ast} values and their standard deviation σ :

$$q_{ass} = 3.262; \sigma = 1.821$$

Similar calculations for long-period comets yield:

$$g_{axit} = 2.296; \sigma = 1.962$$

The normalized difference between these values is:

$$T = (3.262 - 2.296)/\left(1.821^2/171 - 1.962^2/1495\right)^{0.5} = 6.52$$

and its statistical significance exceeds 0.99 [2]. Therefore, based on the qavr parameter, Damocloids exhibit a more than significant advantage over long-period comets. However, it remains unclear how observational selection effects influence this distribution. Clearly, comets having smaller heliocentric distances exhibit greater activity and are easier to detect. Another factor potentially affecting the observed distributions of Damocloids and LPCs is evolutionary in nature. It may be assumed that Damocloids with relatively smaller perihelion distances have depleted their volatile components over long evolutionary timescales, transforming into meteoroid streams. In contrast, observed LPCs likely have undergone fewer passages through the inner Solar System.

6. COMPARISON OF THE ORBITAL INCLINATIONS OF THE TWO SYSTEMS OF CELESTIAL BODIES

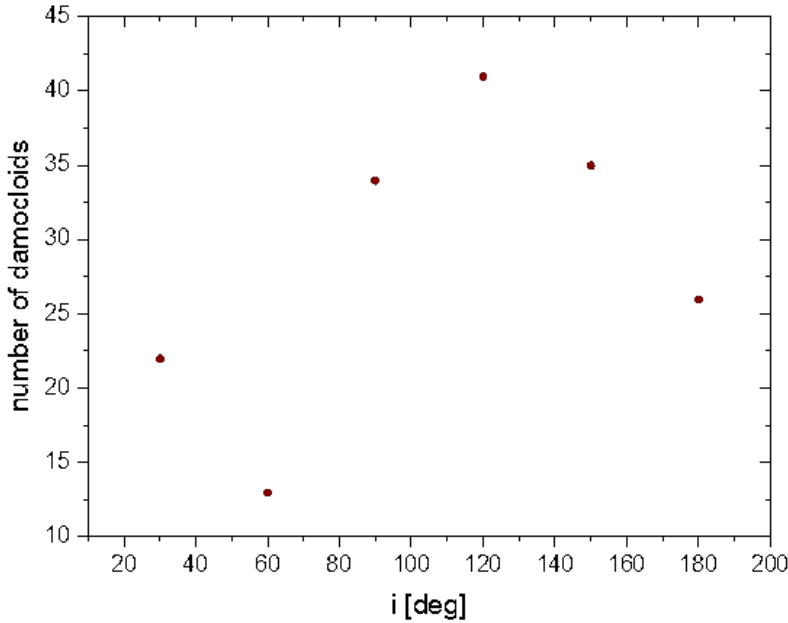The distribution of orbital inclinations for LPCs from the compiled list is shown in Figure 1. The number of prograde and retrograde orbits is 735 and 760, respectively.
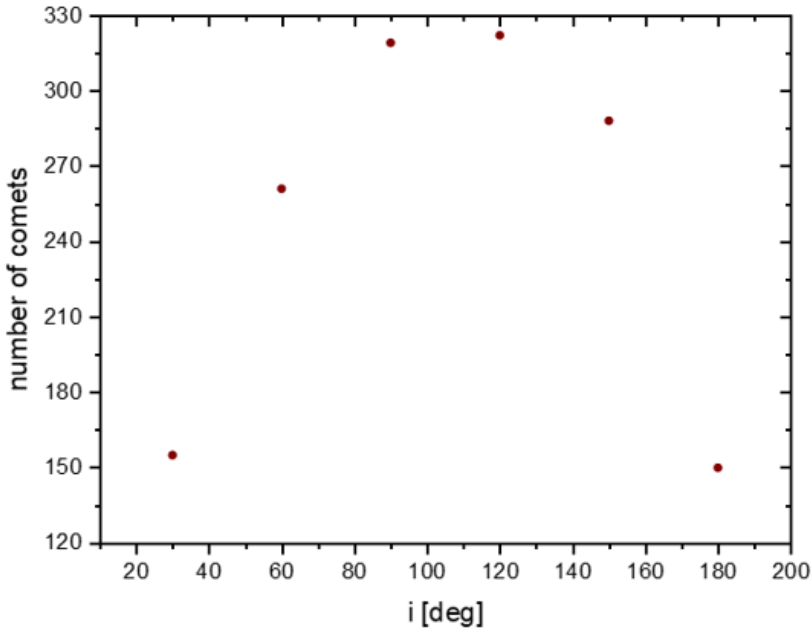
Fig. 1. Distribution of orbital inclinations for 1495 long-period comets.

A dominance of retrograde orbits over prograde ones (102 versus 69) is also observed among Damocloids (Fig. 2). Moreover, this effect is even more pronounced

for Damocloids than in the case of LPCs. Overall, these two distributions are similar to each other. The only observable divergence occurs near $50°$.

Fig. 2. Distribution of orbital inclinations for 1495 long-period comets.

7. DISTRIBUTION OF MOID VALUES FOR DAMOCLOIDS.

Numerous studies have been devoted to investigating the MOID values of long-period comets. However, the most significant numerical characteristics in this area were obtained in [7]. The results from the cited work indicate that the distribution of MOID values for Damocloids relative to the orbits of the giant planets exhibits significant excesses in the low-value range (1.4–1.7 times above the norm), which cannot be explained by random deviations. This implies that a portion of these objects is dynamically linked to the giant planets. In this regard, Damocloids also attract considerable interest. Using algorithms described in [1, 11, 12], we conducted a MOID analysis for 171 Damocloid orbits. Simultaneously, similar calculations were performed for the orbits of long-period comets, since their number increased significantly after publication [8] (1495 versus 1360). Below, we present comparative results for Damocloids and giant planets examined individually within the framework of the research problem:

7.1. Case of Jupiter:

The number of MOID values (ρ) not exceeding 0.322 AU (where ρ is the planetary sphere of influence) is 206 , i.e., 13.8%. The number of Damocloids with similar characteristics is 26 , i.e., 15.2%. When employing threshold values of ρ equal to 0.286 AU and 0.01 AU , the prevalence of Damocloids over LPCs is 1.28 and 15 times, respectively.

7.2. Case of Saturn:

Here, the number of suitable values ($\rho = 0.364AU$) is 18 , i.e., 10.5% for Damocloids. For LPCs, the corresponding number is 135 (9%). By adjusting the ρ threshold to 0.32 AU , the prevalence of Damocloids increases to 1.66 times.

7.3. Case of Uranus ($\rho = 0.346AU$) :

The number of Damocloids is 8 (5%), compared to 61 LPCs (4.1%). Reducing the ρ threshold to 0.32 AU yields a Damocloid predominance to 1.30 times.

7.4. Case of Neptune ($\rho = 0.58AU$)

:

The number of relevant Damocloids is 10(5.8%), and for LPCs, it is 68(4.5%). In this case, Damocloids exhibit a superiority factor of 1.29 .

Thus, in all examined cases, Damocloids dominate LPCs according to this indicator. However, their dominance becomes even more significant if the threshold values are adjusted within reasonable limits.

8. CONCLUSIONS

Damocloids have statistically significantly larger perihelion distances compared to long-period comets.

Unlike long-period comets, Damocloids tend to cluster their orbital perihelia near the ecliptic; however, the perihelion longitudes of Damocloids do not differ from those of LPCs.

Based on their orbital characteristics, Damocloids appear to have undergone considerably more passages through the inner Solar System, particularly within the occupied by giant planets, compared to LPCs.

Dynamical parameters of Damocloids are less effective than those of LPCs for theoretical searches of undiscovered planets in the Solar System. However, the local maxima observed in the 100–120 AU range in both systems constitute an

exception, as they are also accompanied by concentrations of aphelia near two planes with similar parameters.

9. ACKNOWLEDGEMENTS

REFERENCES

1. Gronchi G.F., 2005, Celest. Mech. Dyn. Astron., **93**, 295

2. Gmurman B.E., 2003, Probability Theory and Mathematical Statistics. M.Visha Sola., 479

3. Guliyev A.S., 1992, AstL, 18, **23**, 82

4. Guliyev A.S., 1993, Cosmogonic characteristics of periodic, intermediate and long-period comets. Abstract of the doctoral dissertation.Kyiv

5. Guliyev A.S., 1996, KPCB, **3**, 123

6. Guliyev A.S., Guliyev R.A., 2019, AcA, 69, **2**, 177

7. Guliyev A.S., & Guliyev R.A., 2020, AstL, 46, **10**, 702

8. Kovalenko N.S., Guliyev R.A., Kleshchonok V.V., Guliyev A.S., 2024, AzAJ, **19**, 67

9. Marsden B.G., Williams G.V., 2008, Catalogue of Cometary Orbits$//17^{th}$ edition. Cambridge. SAO, 207

10. Smirnov N.V., 1970, Teorija verojatnostej i matematicheskaja statistika. Izbrannye trudy. –M.:Nauka, 289

11. Tancredi G., 2014, Icarus, **234**, 66

12. Wisniowski T., & Rickman H., 2013, AcA, **63**, 293

)

SCIENTIFIC LEGACY OF PROFESSOR GUSEINOV OKTAY HANGUSEIN

S. O. Guseinova [a*]

[a] *Institute of Physics of Ministry of Science and Education of the Republic of Azerbaijan, Baku, Azerbaijan*

Professor Oktay Guseinov is an outstanding astrophysicist, Doctor of Physical and Mathematical Sciences. Oktay Guseinov is the founder of relativistic astrophysics in the Republic of Azerbaijan and established the first scientific school in this area in Azerbaijan. After graduating from university in 1963, O.Guseinov began his scientific career under the guidance of the world-renowned scientist, physicist, and physical chemist Academician Yakov Borisovich Zeldovich in Moscow. Three-time Hero of the Soviet Union, Ya.B.Zeldovich was one of the creators of the atomic and hydrogen bombs and the famous Soviet rocket "Katyusha". He was a student of Lev Landau. O.Guseinov was fortunate to interact and work with such a brilliant scientist and his circle. As a result of his scientific activities, O.Guseinov made significant contributions to astrophysics, radio, and X-ray astronomy - contributions that play an important role in the development of these fields of modern science. He had foresight in science; relying on his knowledge, he could predict what might be occurring in space. With the advancement of technology, observational data confirmed the reality of the objects and scientific phenomena predicted by O.Guseinov. It is enough to list some of them to understand the magnitude of his scientific legacy.
Keywords: Supernova Remnants – Radiative SNRs – Radio emission

1. NEUTRINO ASTROPHYSICS

Ya. B. Zeldovich and O.H. Guseinov calculated in 1964-1965 what the flux and energy of neutrinos emitted from a star as a result of an explosion in our Galaxy should be. They also proposed that these neutrinos could potentially be detected using existing neutrino telescopes.

* E-mail: gseva703@gmail.com

Fig. 1. Prof Guseinov O.H.

- Ya.B. Zeldovich, O.H. Guseinov - "Neutronization of matter during collapse and the neutrino spectrum" Doklady AN SSSR, v.162, No.4, 1965 [17]

- Ya.B. Zeldovich, O.H. Guseinov - "Neutronization of He-4" J. Exs. Theor. Phys., Letters, 1, 11, 1965 [20].

From 1966 to 1968, Oktay Guseinov analyzed the collapse of hot stars, stating that antineutrinos are also important, and during the explosion, the energy of neutrinos and antineutrinos could be higher than previously calculated.

- O.H. Guseinov - "On experimental possibilities of detection of the collapsed stars" Aston. J., v.43, p.772, 1966; Sov. Astron., v.10, p.613, 1968 [3,4].

- O.H. Guseinov - "Neutrino radiation during stellar collapse" Astron. J., v.45, No.5, 1968; Soviet Astronomy, v.12, p.783, 1969 [4,5].

In 1987, the explosion of a massive star was recorded in the Large Magellanic Cloud. The energy and flux of antineutrinos detected by Japanese and American neutrino telescopes matched the values predicted by Ya. B. Zeldovich and O.H. Guseinov. The observed particles were indeed the antineutrinos that should have been produced in the stars explosion, as Guseinov predicted. Zeldovich and Novikov noted that this idea belonged to Guseinov (Uspekhi Fizicheskikh Nauk, 1965, 86, No. 3, 473) [21].

Japanese scientist Masatoshi Koshiba, using the Super-Kamiokande II neutrino telescope, and American R. Davis were able to detect particles from the explosion. They were awarded the Nobel Prize in 2002 for these observations. American scientists Prof. V. Trimble and Prof. P. Leonard also wrote on this

topic (PASP 1996. 108, pp. 8-34) [16]. "We were struck by two scientists, such as Zeldovich and Guseinov (in 1965), who predicted the neutrino flux from a supernova explosion caused by collapse, and Guseinov (in 1966), who predicted that, despite the neutrino background from past explosions, antineutrinos from the collapse could be at an observable level"

2. THE NECESSITY OF SEARCHING FOR NEUTRON STARS AND BLACK HOLES IN CLOSE BINARY SYSTEMS AND THEIR STRONG X-RAY SOURCES

Ya. B. Zeldovich and O.H. Guseinov showed that the components of X-ray sources could be neutron stars or black holes and described in 1965 how to observe these stars. In 1970, O.H. Guseinov, in his paper, explained what the properties of neutron stars, black holes, and binary star systems might be.

- Ya.B. Zeldovich, O.H. Guseinov - "Collapse of stars in binaries," Astrophys. J., v.144, p.840, 1966; Astron. J., No.2, 1966. [18, 19]

- O.H. Guseinov - "X-ray source in binaries", Sov. Aston. 1970, 47, 1143. [6]

It was necessary to search for neutron stars and black holes in close binary stars, which are powerful sources of X-ray emission, using telescopes located on satellites in space. The first orbital X-ray telescope, UHURU, was launched in 1971, and after the satellite began operation, the ideas and predictions of O.H. Guseinov were confirmed, with the discovery of X-ray pulsars. In I. Novikov's book "HOLES IN SPACE AND TIME" (2006, p.112) [14], it is stated: "I want to emphasize that the organization of the search for relativistic objects in the Universe was initiated in 1965 by Yakov Zeldovich and Oktay Guseinov" Andrew G. Lyne and Francis Graham-Smith in their book "PULSAR ASTRONOMY," Cambridge University Press, 1998. It was noted: "Compact stars, whether white dwarfs or neutron stars, were predicted as observable sources of X-rays. In 1964, the predictions were made by Zeldovich and Guseinov." M. Longair, in his book "THE NEW COSMIC CENTURY: A HISTORY OF ASTROPHYSICS AND COSMOLOGY" (2006, p. 199) [12], writes: "in 1965, Yakov Zeldovich and Oktay Guseinov proposed that the observation of X-rays or γ -rays from spectroscopically single-lined binary systems could indicate either a neutron star or a black hole."

Riccardo Giacconi led the scientific programs of the orbital X-ray telescope "UHURU" and was awarded the Nobel Prize in 2002 for finding X-ray sources using the satellite.

O.H. Guseinov recalled the work [6, 7] while in Turkey: "Before 1971, it was not even known whether X-ray sources were point-like, as the uncertainty in their

coordinates could be as large as 4-5 degrees. To determine what these sources were and to identify which optical star they were a component of, it was necessary to understand the characteristics of X-ray and optical bands of the binary X-ray sources we predicted. I sent this work to a journal in 1967, but because the results seemed incredible and the work appeared too early, it was only published in 1970."

O.H. Guseinov, K.I. Novruzova - "Collapsed Stars in Binary Systems" Astronomicheskii Zhurnal, Vol. 48, p.221; Soviet Astronomy, Vol. 15, p.173, No.1, p.173, 1971 [9, 10]

3. RADIO AND X-RAY ASTROPHYSICS

In 1966, Oktay Guseinov and Pavel Amnuel, predicted that certain celestial bodies could emit periodic X-rays, even before the first pulsars were discovered. Six months later, in the UK, an astrophysical group led by Antony Hewish at Cambridge recorded an unexpected, regularly repeating signal during research on radio emissions in the interplanetary medium.

- P.R. Amnuel, O.H. Guseinov -"X-rays during the accretion of interstellar matter" Izvestiya AN Azerb. SSR, No. 3, 1968. [1]

- P.R. Amnuel, O.H. Guseinov -"The influence of interstellar medium parameters on accretion by neutron stars" Astron. Nachr., v. 294, p. 139, 1972. [2]

For the detection of the signal using the meridian radio telescope, Hewish was awarded the Nobel Prize in 1974.

As a result, the astrophysical objects predicted in advance by O.H. Guseinov, representing our country, have been found in galaxies, and the scientific events have been confirmed. Those who confirmed these findings through their observations were awarded the Nobel Prize:

1. Japanese Masatoshi Koshiba, American R. Davis in 2002.

2. English Antony Hewish in 1974.

3. Italian Riccardo Giacconi in 2002.

Of the six Nobel Prizes awarded in cosmology up to 2002, three were related to the research conducted by Professor Oktay Guseinov, whose significant predictions have secured his place in the history of global cosmology.

Professor V.M. Lipunov noted in his book "Astrophysics of Neutron Stars" (Springer-Verlag, 1992, p.6) [11]: "A significant ideological and psychological barrier was overcome by Soviet scientists Amnuel and Guseinov (in 1968), who pointed out the necessity of considering the magnetic field of neutron stars. From general considerations, it follows that neutron stars should have strong magnetic fields, and the accreting matter under realistic conditions is a good conductive plasma. The way in which matter falls onto the star can change dramatically in a magnetic field. How matter falls onto the star can change dramatically in a magnetic field. Thus, even spherical accretion near neutron stars can lead to anisotropy in the distribution of matter and, consequently, radiation. As a result of the rotation of neutron stars, the radiation appears to the observer as periodically pulsing."

These objects were named "PULSARS". The discovery of the pulsar was perceived as the beginning of a new era in astrophysics. Professor V.M. Lipunov noted in "Astrophysics of Neutron Stars" (Springer-Verlag, 1992, pp. 11-12) [11]: "All publications regarding the theory of neutron star accretion prior to the launch of the Uhuru satellite were made by Soviet scientists:

1. Novikov, Zeldovich 1966;

2. Shklovskiy 1967;

3. Amnuel, Guseinov 1968;

4. Zeldovich, Shakura 1969;

5. Bisnovaty-Kogan, Fridman 1969;

6. Amnuel, Guseinov 1969;

7. Guseinov 1970;

8. Shvartsman 1970, 1971;

9. Amnuel, Guseinov 1972;

10. Shakura 1972.

4 out of 10 on this topic were completed by Azerbaijani scientists working at the Shamakhi Astrophysical Observatory during those years.

Professor Malcolm Longair, Royal Astronomer of Scotland, Director of the Royal Observatory in Edinburgh, and Vice-President of Clare Hall College at Cambridge, published a book in 2006 titled "THE NEW COSMIC CENTURY: A HISTORY OF ASTROPHYSICS AND COSMOLOGY" [13].

In this book, he discusses the most important scientific achievements from 1900 to 2000 and lists the names, surnames, and years of life of the authors of these results. It should be noted that the Azerbaijani Oktay Guseinov is the only scientist from Turkic-speaking countries recognized in this book, and his scientific achievements are examined in detail.

In 1987, a group of academicians from the Academy of Sciences of the USSR published a book that compiled information about the greatest achievements in Soviet science and technology from 1917 to 1987: "THE GREATEST ACHIEVE-MENTS OF SOVIET SCIENCE AND TECHNOLOGY FROM 1917 TO 1987" [15].

Only two individuals of Turkic origin from the former USSR were mentioned in this book: the Azerbaijani astrophysicist Oktay Guseinov and the oilman Emin Taghiyev.

The Shamakhi Observatory held a special place in O.H.Guseinov life, where he worked from 1966 to 1982. He headed the Department of Theoretical Astrophysics, served as Deputy Director, and later as Director of the Observatory. From 1982 to 1992, he headed a laboratory at the Institute of Physics of the Azerbaijan National Academy of Sciences. In April 1992, Oktay Guseinov moved to Turkey at the invitation of the Faculty of Science at METU. By the initiative of the then-president of TUBITAK Professor Dr. Tosun Terzioglu, in 1995, Guseinov became a Turkish citizen with the "special status of a distinguished scholar."

4. CONCLUSIONS

Guseinov was the first to propose a method for searching for black holes in binary systems that were previously unobservable, and he compiled a list of such objects. Under his guidance, several catalogs were published, including: -

- A Complete Catalog of Galactic Supernova Remnants

- A catalog of X-ray sources

- A catalog of white dwarfs

- A catalog of pulsars

Over his 45 years of scientific activity, O.H.Guseinov published more than 300 scientific articles in leading international journals, which have been cited over 1200 times, and these citations continue to this day. Professor O.H. Guseinov is the author of four monographs. He was a person who lived for science. Oktay Guseinov trained young specialists who successfully worked and continue to work in Azerbaijan, Turkey, the USA, and Europe.
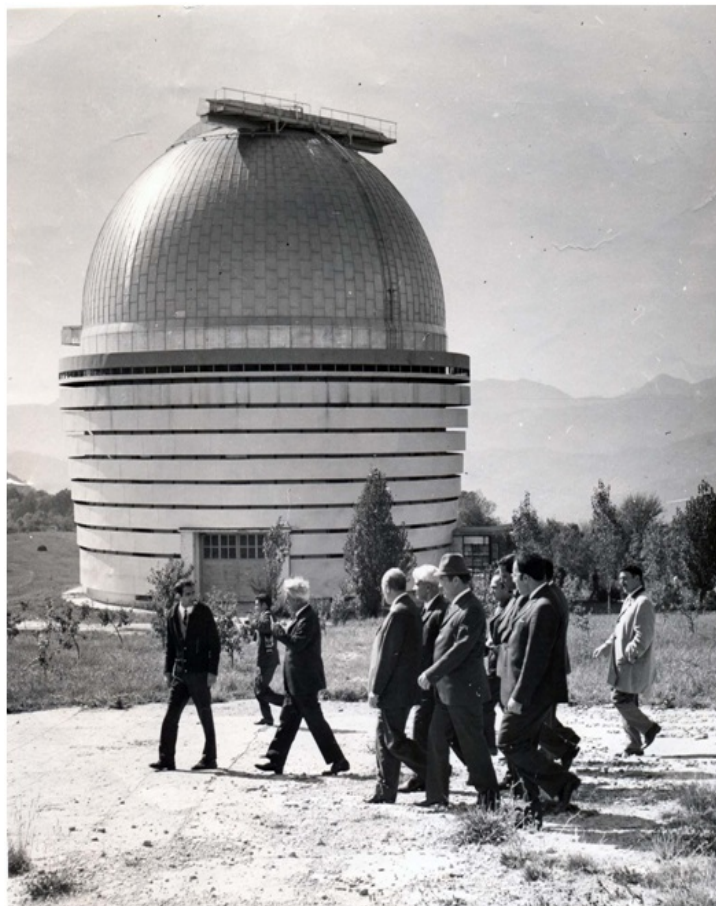
Fig. 2. O.H.Guseinov demonstraits the telescope

At various universities he courses given for Master of Science and Doctor of Philosophy: Astrophysics, General Physics, Thermodynamics, Statistical Physics, Atomic and Nuclear Physics, Particle Physics, Special and General Theory of Relativity, Electromagnetic Theory, High Energy Physics and Astrophysics, Special Studies in Physics.

He was awarded two medals from the USSR, was the author of two patents registered in the Russian Federation, and actively participated in numerous international scientific conferences. A full member of the International Astronomical Union, Guseinov continued his scientific work after retiring. He worked on publishing books in physics:

1. Molecular physics, thermodynamics, and statistical physics (primarily statistical physics);

Fig. 3. O.H.Guseinov with Sultanov G., Keldysh M. and Bagirov G.

2. Classical field theory (including electrodynamics, special and general relativity);

3. Atomic and nuclear physics (with a section on particle physics totaling 30-40 pages).

Additionally, he prepared materials for a question-and-answer format book that would interest schoolchildren, students, and the general public. He also published popular articles on various topics, which was his hobby.

- The Effect of Global Warming on Human Life and Thought

- We're done with Darwin, is it Einstein's turn?

- Universe, Allah, Evolution and Islam -1, 2.

- Wrongly Taught Physics: An Example.

Fig. 4. Memorial meeting at the Institute of Physics.

- If Einstein were in an Underdeveloped Country?

- If Einstein were in Turkey?

- Why Are We Behind in Science?

- Evaluation of Articles by Those Working for Good Physics Education.

- Cheap Ways to Go to Siberia.

- European Union.

- Contribution to Science and Contribution of Some Turkish Scholars to Science.

- Our Opportunity to Contribute to Scientific Thought, Physics Education and Physics Science.

- Brief History of Hydrogen and Neutron Bomb Production in the Soviet Union.

- Genetic Weapons.

- The Ladder or Stick Issue in High School.

- Scalar and Vector Quantities.

- Why aren't Anthills Flooded?

- Nobel Prizes in Physics

and so on.

A book dedicated to the spouses of O.H. Guseinov and his students E. Yazgan and A. Ankay was published in the USA in 2007: "Neutron Stars, Supernovae, and Supernova Remnants" Nova Science Publishers - New York [8].

Oktay Guseinov passed away on March 25, 2009, at his home in Turkey and was buried in the Undjaly cemetery in Antalya.

REFERENCES

1. Amnuel P.R. & Guseinov O.H., 1968, Izvestiya AN Azerb. SSR, 3

2. Amnuel P.R. & Guseinov O.H., 1972. Astron. Nachr., **294**, 139

3. Guseinov O.H., 1966, Aston. J., **43**, 772

4. Guseinov O.H., 1968, Sov. Astron., **10**, 613

5. Guseinov O.H., 1969, Soviet Astronomy, **12**, 783

6. Guseinov O.H., 1970, Sov. Aston., **47**, 1143

7. Guseinov O.H., 1968, Astron. J., **45**, 5

8. Guseinov O.H., Askin A., & Yazgan E., 2007,"Neutron stars, supernovae, and supernova remnants" Nova Science Publishers, (ISBN: 1-60021-548-3)

9. Guseinov O.H., & Novruzova K.I., 1971, Astron. J., 1, **15**, 173

10. Guseinov O.H., & Novruzova K.I., 1983, Astron. Zhur., **48**, 221

11. Lipunov V.M., 1992 "Astron J", Springer-Verlag, 6

12. Longair M., 2006, Jour. Mod. Phys.,199

13. Loren R.S, 1987, Historty of Science Soe .New.,**184**, 15

14. Novikov I.D., Holes in space and time, 2006, 356

15. The greatest achievements of soviet science and technology from 1917 to 1987 (in russian), 1987

16. Trimble V. & Leonard P., 1996, PASP, **108**, 8

17. Zeldovich Ya.B & Guseinov O.H., 1965, Dok. AN SSSR, **162**, 4

18. Zeldovich Ya.B & Guseinov O.H., 1966, Astron. J., **2**,112

19. Zeldovich Ya.B & Guseinov O.H., 1966, Astrophys. J., **144**, 840

20. Zeldovich Ya.B & Guseinov, O.H.,1965 J. Exs. Theor. Phys., Letters, **1**, 11

21. Zeldovich Ya.B & Novikov, I.D., 1965, Uspekhi Fizicheskikh Nauk, 86, **473**, 3